Seasonal and spatial variations of greenhouse gas (CO_2, CH_4 and N_2O) emissions from urban ponds in Brussels

Bauduin T.[1,2,*], Gypens N.[1], Borges A.V.[2]

[1] Ecology of Aquatic Systems, Free University of Brussels, Belgium

[2] Chemical Oceanography Unit, University of Liège, Belgium

[*] thomas.bauduin@ulb.be

Highlights :

- First survey of GHG emissions from Brussels ponds
- Small ponds are more subject to edge effects and have higher pCO_2
- Macrophytes enhance methane production in ponds
- City center ponds have higher N_2O emissions due to atmospheric deposition
- Brussels ponds emissions were equivalent to the carbon sink estimated for the urban green spaces.

Seasonal and spatial variations of greenhouse gas (CO_2, CH_4 and N_2O) emissions from urban ponds in Brussels

Bauduin T.[1,2,*], Gypens N.[1], Borges A.V.[2]

[1] Ecology of Aquatic Systems, Free University of Brussels, Belgium

[2] Chemical Oceanography Unit, University of Liège, Belgium

[*] thomas.bauduin@ulb.be

Abstract:

Freshwaters have been recognized as important sources of greenhouse gases (GHG) to the atmosphere. However, urban ponds have received little attention even though their number is increasing due to expanding urbanisation globally. Ponds are frequently associated to urban green spaces that provide several ecosystemic services such as cooling local climate, regulating the water cycle, and acting as small carbon sinks This study aims to identify and understand the processes producing GHGs (CO_2, CH_4, and N_2O) in the urban ponds of the temperate European city of Brussels in Belgium. 22 relatively small ponds (0.1-4.6 ha) surrounded by contrasted landscape (strictly urban, bordered by cropland or by forest), were sampled during four seasons in 2021-2022. The mean ± standard deviation was 3,667 ± 2,904 ppm for the partial pressure of CO_2 (pCO_2), 2,833 ± 4,178 nmol L^{-1} for CH_4, and 273 ± 662 % for N_2O saturation level ($\%N_2O$). Relationships of GHGs with oxygen and water temperature suggest that biological processes controlled pCO_2, CH_4 concentration and $\%N_2O$. However, pCO_2 was also controlled by external inputs as indicated by the higher values of pCO_2 in the smaller ponds, more subject to external inputs than larger ones. The opposite was observed for CH_4 concentration that was higher in larger ponds, closer to the forest in the city periphery, and with higher macrophyte cover. N_2O concentrations, as well as dissolved inorganic nitrogen, were higher closer to the city center, where atmospheric nitrogen deposition was potentially higher. The total GHG emissions

from the Brussels ponds were estimated to 1kT CO_2-eq per year and were equivalent to the carbon sink of urban green spaces.

Keywords:

carbon dioxide, methane, nitrous oxide, Brussels, urban ponds, urban ecology, macrophytes

1. Introduction

The three main greenhouse gases (GHGs) emitted to the atmosphere by human activities are carbon dioxide (CO_2), methane (CH_4) with a global warming potential (GWP) 34 times greater than CO_2 on a 100-year time scale, and nitrous oxide (N_2O) with a GWP 298 times greater than CO_2 on a 100-year time scale (Myrhe et al., 2013). In inland waters, the production of CO_2 and CH_4 are mainly due to the degradation of organic matter (OM) through mainly aerobic processes for CO_2 (Del Giorgio et al., 1999; Cole and Caraco, 2001) and by anaerobic archaeal methanogenesis for CH_4 (Conrad, 2020). The OM in inland waters can be autochthonous or allochthonous. Autochthonous production of OM is from phytoplankton (McClure et al., 2020; Bartosiewicz et al., 2021) or aquatic macrophytes (Grasset et al., 2019; Desrosiers et al., 2022). The relation between autochthonous biomass (phytoplankton and macrophytes) and CH_4 emissions is well established (DelSontro et al., 2018; Borges et al., 2022; Bastviken et al., 2023). The impact of autochthonous biomass on CO_2 depends on the phase of the bloom development, high concentrations of chlorophyll-*a* (Chl-*a*) during the growth and peak phases coinciding with intense photosynthesis and CO_2 consumption (Grasset et al., 2020; Borges et al. 2022;), and phases of senescence leading to CO_2 production. Allochthonous OM in small water bodies (e.g., ponds) comes from fallen leaves of the surrounding vegetation and from particulate and dissolved OM from surface runoff or from soil-water and groundwater inputs (Gasith and Hosier, 1976; Weyhenmeyer et al., 2015). The N_2O production is mainly due to microbial nitrification and denitrification and is dependent on the availability of dissolved inorganic nitrogen (DIN) and O_2 (Codispoti and Christensen, 1985; Mengis et al., 1997). Anthropogenic nitrogen inputs from leakage of fertilizers from croplands or from atmospheric deposition may enhance the N_2O emissions in freshwater wetlands, lakes and rivers (McCrackin & Elser, 2011; Bettez & Groffman, 2013; Sønderup et al., 2016; D'Acunha et al., 2019; Decina et al., 2020; Bonetti et al., 2022).

The emissions from inland waters (rivers-streams, lakes and reservoirs) of GHGs were estimated at 14.3 Pg CO_2 yr^{-1} for CO_2 (Drake et al., 2018), 6.03 Pg CO_2 equivalent (CO_2-q) yr^{-1} for CH_4 (Rosentreter et al., 2021) and 0.05 Pg CO_2-eq yr^{-1} for N_2O (Lauerwald et al., 2019). Yet, these estimates remain highly uncertain because of the low number of measurements that is insufficient to account for the strong spatial and temporal variability of the fluxes within a given system, as well as the high diversity of systems due to differences in size, climate, catchment morphology, land cover, and anthropogenic pressures.

Several studies have shown the importance of small water bodies (surface area < 0.1 ha) as hotspots for GHG emissions (Holgerson and Raymond, 2016; Grinham et al., 2018; Rosentreter et al., 2021; Peacock et al., 2021). Although only representing 9% of the total area of lentic waters, small water bodies account for 15% and 40% of diffusive emissions from lakes of CO_2 and CH_4, respectively according to Holgerson and Raymond (2016). Urban areas have a large number of small water bodies in the form of ponds mostly associated to green spaces such as public parks, and their number is increasing due to rapid urbanisation worldwide (Brans et al., 2018; Audet et al., 2020). Yet, only a very limited number of studies have investigated GHG emissions from urban ponds (Singh et al., 2000; Natchimuthu et al., 2014; van Bergen et al., 2019; Audet et al., 2020; Peacock et al., 2021). Urban ponds are small and thus have high ratio of perimeter to surface area (Hanson et al., 2007), surrounded by impervious surfaces (Davidson et al., 2015; Peacock et al., 2021), and a high stormwater runoff that combined result in high inputs of OM and DIN that should sustain emissions of CO_2, CH_4, and N_2O to the atmosphere. Additionally, urban ponds are usually very shallow so there is a strong influence on the water column of GHG production in sediments.

Brussels is the most densely populated area in Belgium and the largest city of the country and contains 158 ponds totalling a surface area of 101ha. The population is more than 1 million inhabitants, equating to less than $1m^2$ of water body per inhabitant, indicating a high degree of anthropogenic pressure on these ecosystems. However, not all urban ponds are subject to the same degree of anthropogenic pressure, as the periphery of the city is bordered by cropland and forest. Yet, the ponds in Brussels are highly eutrophied with in some cases high algal biomass but also macrophytes which compete with phytoplankton for nutrients (Peretyatko et al., 2007 ; de Backer et al., 2010 ; Peretyatko et al., 2012 ; Descy et al., 2016). Yet, the equilibrium between the prevalence of macrophytes and phytoplankton entails a gradual shift rather than an abrupt process and is influenced by additional factors other than nutrient levels (Van Nes et al., 2002; Davidson et al., 2023). It can be

hypothesized that water bodies with a dominance of phytoplankton and a dominance of macrophytes should have different GHG dynamics, although this has seldom been tested (Harpenslager et al., 2022 ; Baliña et al., 2023).

Here, we report CO_2, CH_4, and N_2O dissolved concentrations and complementary variables (water temperature, chlorophyll-*a* (Chl-*a*), DIN, and O_2) sampled in 22 small urban ponds (0.1-4.6 ha) of the city of Brussels, during the four seasons in 2021-2022. Potential drivers of CO_2, CH_4, and N_2O dynamics are investigated by comparing pond size, presence of macrophytes, relative distance to the city center, surrounding landscape (strictly urban, bordered by cropland or by forest). We test if the most frequent accepted hypotheses of the drivers of CO_2, CH_4 and N_2O seasonal and spatial variations in natural lakes and ponds also apply to urban ponds The CO_2, CH_4, and N_2O diffusive emissions are computed and compared to the official inventory of GHG emissions from the city of Brussels.

2. Material and methods

2.1. Pond selection and sampling frequency

22 ponds were selected within the Brussels region (Fig. 1). All of the ponds are artificial and were built during the past century, the majority with the primary aim of landscaping and embellishing parks. Recreational fishing activities are allowed in four of the sampled ponds (Table S1). Some of the sampled ponds are connected to a river network (flow-through ponds) and others are fed directly by groundwater and small watercourses (overflow ponds), where water level is kept constant by an overflow outlet (Table S1). The sampled ponds are in the four main catchment areas of the city of Brussels (Molenbeek (n=2), Neerpedebeek-Vogelzangbeek (n=4), Maelbeek (n=6), and Woluwe (n=10) catchments) (Table S1). Four sampling campaigns were carried out on the 22 ponds, corresponding to the four seasons: November 2021 (Fall), February 2022 (Winter), May 2022 (Spring) and August 2022 (Summer).

2.2. Meteorological data

Air temperature, rainfall and wind speed were retrieved from https://wow.meteo.be/fr for the meteorological station of the Royal Meteorological Institute of St-Lambert (50.8408 °N, 4.4234 °E) in Brussels, located between 1 and 10 km from the sampled ponds. Wind speeds and air temperatures were averaged over 24 hours to obtain a daily average value. The rainfall was integrated on each day to obtain the daily rainfall.

2.3. Sampling in field

Water was sampled and collected from pontoons. Water pH, temperature, conductivity and oxygen saturation level (%O_2) were measured by a VWR MU 6100 H probe. Water was collected in 2L polypropylene bottles for subsequent sampling for Chl-*a*, total suspended matter (TSM) and dissolved inorganic nutrients (ammonium (NH_4^+), nitrite (NO_2^-), nitrate (NO_3^-), soluble reactive phosphorus (SRP)). Three 50mL falcon tubes were filled with unfiltered water to which was added 200µL of HNO_3 (65%) for total phosphorus (Ptot) analysis.

Macrophytes were defined as vascular aquatic plants, excluding filamentous algae, mosses and liverworts, (Bowden et al., 2017). The percentage of macrophyte cover was estimated visually during sampling. Dominant species of macrophytes (*Potamogeton pectinatus, Ceratophyllum demersum, Chara sp., Nitella sp., Lemna trisulca, Zannichellia palustris*) were identified in August 2022, when macrophyte cover was maximal. This list of species of macrophytes agreed with past studies in Brussels ponds (Peretyatko et al., 2009; de Backer et al., 2010).

2.4. Laboratory analysis

Water was filtered on Whatman filters 0.7µm GF/F glass microfibers with diameter of 47mm for TSM and Chl-*a* (stored frozen). Filtered water was stored in 50 ml plastic vials and stored frozen for dissolved nutrients analysis. Chl-*a* was measured on extracts with 90% acetone by fluorimetry (Kontron SFM 25 model) (Yentsch and Menzel, 1963). NH_4^+ was determined with the nitroprusside-hypochlorite-phenol coloration method (Grasshoff and Johannsen, 1972). NO_2^- and NO_3^- were determined before and after reduction of NO_3^- to

158 NO_2^- by a cadmium-copper column, with Griess' reagent in acidic medium coloration method
159 (Grasshoff et al., 1983). SRP was determined with ammonium molybdate, ascorbic acid and
160 potassium antimony tartrate coloration method (Koroleff, 1983).

161 Ptot was determined by inductively coupled plasma spectroscopy (ICP) on an ICP-
162 OES Perkin Elmer Avio 200 model. The assay protocol was based on the US EPA (1994)
163 method 200.7 for analysis of metals and trace elements in water by ICP with prior microwave
164 acid digestion based on US EPA, (2007) method 3015A.

165

166 **2.5. Measurement of GHG concentrations and computation of fluxes**

167

168 CO_2 measurements were carried out on the field with a Li-Cor Li-840 CO_2/H_2O gas
169 analyser using the headspace technique with 4 polypropylene syringes of 60mL. The
170 technique consisted in equilibrating inside the syringe 30mL of sample water with 30mL of
171 atmospheric air by vigorous shaking during 5 minutes. The headspace of each syringe was
172 injected sequentially in the Li-840 and a fifth syringe was used to measure atmospheric CO_2.
173 The final pCO_2 value was computed taking into account the partitioning of CO_2 between
174 water and the headspace, as well as equilibrium with HCO_3^- (Dickson et al. 2007) using
175 water temperature measured in-stream and after equilibration, and total alkalinity (data not
176 shown). Samples for total alkalinity were conditioned, stored and analysed as described by
177 Borges et al. (2019). The Li-Cor Li-840 was calibrated before and after each sampling period
178 with ultrapure N_2 and a suite of gas standards (Air Liquide Belgium) with CO_2 mixing ratios
179 of 388, 813, 3788 and 8300 ppm. The overall precision of pCO_2 measurements was ±2%.

180 Samples for dissolved CH_4 and N_2O were collected directly in surface waters with 60
181 ml plastic syringes and transferred with a plastic tube into two 60mL borosilicate serum
182 bottles and poisoned with 200µL of saturated $HgCl_2$ solution. The vials were sealed with a
183 butyl stopper and crimped with an aluminium cap. Measurements were carried out using the
184 headspace technique with a SRI 8610C gas chromatograph with a flame ionisation detector
185 (FID) for CH_4 and an electron capture detector (ECD) for N_2O, calibrated with CH_4:N_2O:N_2
186 gas mixtures (Air Liquide Belgium) with mixing ratios of 1, 10, 30, 509, and 2010 ppm for
187 CH_4, and 0.2, 2.0 and 6.0 ppm for N_2O. The precision of measurement was ±11% for CH_4
188 and ±6% for N_2O based on 176 replicates. Ebullitive CH_4 fluxes were not measured during
189 this study, but were measured with inverted funnels (e.g. Keller and Stallard, 1994) in four

ponds (Leybeek, Pêcheries Royales, Silex, Ten Reuken) for the period of 29/03/22 to 09/09/23 (unpublished data).

The CO_2 concentration is expressed in terms of partial pressure of CO_2 (pCO_2 in ppm), the CH_4 dissolved concentration in nmol L^{-1} corresponding to the usual convention in topical literature. N_2O concentrations oscillated around atmospheric equilibrium, so the data are presented as a percentage of the saturation level (%N_2O), where 100% corresponds to atmospheric equilibrium. The atmospheric pCO_2 was measured on the field with the Li-Cor Li-840. The equilibrium with atmosphere for N_2O was calculated from the average air mixing ratios of N_2O provided by the Global Monitoring Division (GMD) of the National Oceanic and Atmospheric Administration (NOAA) Earth System Research Laboratory (ESRL) (Dutton and Hall, 2023). A constant atmospheric concentration of 1.9 ppm was assumed for CH_4.

The exchange of CO_2, CH_4, and N_2O between surface water and the atmosphere was calculated according to:

$$F_G = k_g \Delta C$$

F_G (mmol $m^{-2}d^{-1}$) is the flux of a specific gas (G), k_g (cm h^{-1}) is the specific gas transfer velocity, and ΔC is the gas concentration gradient in water and the atmosphere (mmol L^{-1}).

The k_g values were derived from the gas transfer velocity normalized to Schmidt number of 600 (k_{600}) according to :

$$k_g = k_{600} \times (Sc/600)^{-0.5}$$

where Sc is the Schmidt number of the given gas in freshwater at in-situ water temperature computed according the algorithms given by Wanninkhof (1992).

k_{600} was computed from wind speed using the parameterisation of Cole and Caraco (1998):

$$k_{600} = 2.07 + 0.215\, u^{1.7}$$

where u is the wind speed (m s^{-1}).

The average daily u value on the day of sampling of each sampled pond was used. The u data were measured at the meteorological station of the Royal Meteorological Institute of St-Lambert (50.8408 °N, 4.4234 °E) in Brussels (located between 1 and 10 km from the sampled ponds) (retrieved from wow.meteo.be). The area-weighted average of F_G from the 22 sampled ponds (totaling a surface area of 34 ha) for each of the 4 seasons was averaged

to obtain an annual value that was extrapolated to the total surface area (101 ha) of the all of the 158 urban ponds of the city of Brussels.

The emissions of CH_4 and N_2O were expressed in CO_2 equivalents (CO_2-eq) by multiplying the respective fluxes by global warming potential (GWP) values of 34 for CH_4 and 298 for N_2O corresponding to a time horizon of 100 years (Myrhe et al., 2013).

2.6. Statistical analysis

The statistical analyses were conducted using R version 4.1.1 (2022) (R Core Team, 2022) and graphs were produced with GraphPad Prism v9. Prior to analysis, data underwent logarithmic or square root transformations to ensure normality. Shapiro tests were performed to assess the normality of the distribution.

To investigate relationships between variables, quantile regressions were performed with the quantreg package v5.95 (Koenker, 2005). Quantile regressions were chosen over linear regressions due to their ability to provide a more comprehensive understanding of potential causal relationships in ecological processes (Cade and Noon, 2003). Significance levels for the quantile regression were determined using Wald statistical tests.

For comparisons of medians in the boxplots, permutational multivariate analysis of variance (PERMANOVA) on each Bray-Curtis distance matrix with 999 permutations was performed. A post-hoc test was performed to establish significant differences between sample pairs. For multiple comparisons, *p*-values were adjusted using the Bonferroni correction. Simultaneously, a test for homogeneity of multivariate dispersions (PERMDISP) was conducted. This test allowed for the examination of dispersion effects independent of location effects, as significant differences could be attributed to variations in within-group dispersion rather than differences in medians values among the groups (Anderson, 2006). PERMANOVA and PERDISP were performed using the vegan package v2.6.4 (Oksanen et al., 2013).

2.7. Data availability

The time-sampled and georeferenced data-set presented in this paper is publicly available (Bauduin et al., 2024).

3. Results

3.1. Seasonal variations of meteorological conditions and GHGs

In 2022, the average air temperature in Brussels was 12.2°C, above the average of 11.0°C for the 1991-2020 period. With the exception of April, September and December, air temperature monthly averages were above the reference value for the 1991-2020 period. A total of 701 mm of rain fell in Brussels (837 mm for the 1991-2020 period), during 149 days (190 days for the 1991-2020 period). The year 2022 was the fourth driest and the first (ex-aequo with 2020) warmest year of the current reference period. During the sampling period from 22/11/21 to 18/08/22, the air temperature and wind speed averaged 11.9±6.3°C and 0.6±0.6 m s^{-1}, respectively, and the total precipitation was 321mm in the city of Brussels (Fig. 2A). Air temperature was highest in summer (22.2±1.6°C) and lowest in fall (6.1±0.7°C). The highest wind speed was in spring (Fig. 2B) (1.7±0.5 m s^{-1}). In the 15 days prior to sampling, it rained a total of 13mm in fall, 53mm in winter, 13mm in spring, and less than 1 mm in summer.

During the four sampling periods, pCO_2 averaged 3,667 ± 2,904 ppm, CH_4 concentration averaged 2,833 ± 4,178 nmol L^{-1}, and $\%N_2O$ averaged 273 ± 662 % in the 22 sampled ponds in the city of Brussels. The maximum pCO_2 value was observed in fall (15,029 ppm) and the minimum value in summer (121 ppm). Median pCO_2 was higher in fall than during the other seasons and was lower in winter than spring (Fig. 3A). The maximum and minimum CH_4 concentration values were both observed in summer, 29,190 and 10 nmol L^{-1}, respectively (Fig. 3B). The CH_4 concentrations showed seasonal variations, with significantly lower median concentration in winter than other seasons, and higher concentrations during spring and summer (Fig. 3B). The minimum and maximum values of $\%N_2O$ were both observed during summer (0 and 10,354%) (Fig. 3C). The median concentration of $\%N_2O$ was lower during summer than fall and winter. The $\%N_2O$ values showed a higher dispersion during summer than other seasons (Fig. 3C). Undersaturation of CO_2 with respect to atmospheric equilibrium was observed only on 7 occurrences (out of 88 observations), during spring (2 times) and summer (5 times). For N_2O, undersaturation

with respect to atmospheric equilibrium was observed at each season, 3 times in fall, 5 times in winter, 7 times in spring and 10 times during summer. CH_4 concentrations were always above saturation.

The average, median, minimum and maximum values of ancillary variables ($\%O_2$, Chl-*a*, SRP, Ptot, NH_4^+, NO_3^- and NO_2^-) are given in Table S2. The median $\%O_2$ values were significantly lower in fall than in the other seasons (Table S2). The median Chl-*a* concentration value was significantly lower in winter than in fall and the highest concentrations were measured in summer, when values were the most variable. There were no differences between seasons for SRP. Ptot had higher concentrations in spring and summer than in fall and winter. DIN concentrations were significantly higher in fall and winter than during spring and summer. NH_4^+, NO_3^- and NO_2^- concentrations were significantly higher in fall than during the other seasons.

pCO_2, CH_4 concentration and $\%N_2O$ were negatively related to $\%O_2$ (Figs. 4A, 4G, 4M). CH_4 concentration was positively related to water temperature (Fig. 4H) and $\%N_2O$ was negatively related to water temperature (Fig. 4N). There was no relation between pCO_2 and water temperature (Fig. 4B), nor Chl-*a* concentration (Fig. 4C). pCO_2 was positively related to SRP (Fig. 4E). CH_4 was negatively related to Chl-*a* (Fig. 4I). There was a positive correlation between CH_4 and Ptot (Fig. 4L), that was also observed during each individual season, except in winter (Figs. S2A, S2B, S2C, S2D). The negative relation observed between CH_4 and DIN (Fig. 4J) could be spurious and be attributed to parallel seasonal changes of both variables, as there were no correlations between CH_4 and DIN when analysed independently for each season, except in spring (Figs. S2E, S2F, S2G, S2H). $\%N_2O$ was positively correlated to DIN for the whole dataset (Fig. 4P) as well as for each season analysed independently (Figs. S2I, S2J, S2K, S2L). $\%N_2O$ was statistically more strongly correlated to NO_2^- (Fig. 5C) and NO_3^- (Fig. 5D) than to NH_4^+ (Fig. 5B). $\%N_2O$ was negatively related to O_2:DIN (Fig. 5E), O_2:NO_2^- (Fig. 5G) and O_2:NO_3^- (Fig. 5H) but unrelated to O_2:NH_4^+ (Fig. 5F).

3.2. Spatial variations of GHGs

As pond perimeter (r = 0.90, p<0.0001) and depth (r=0.45, p 0.014) were correlated to surface area ; hereafter, only relationships between GHGs and pond surface area are

315 presented (Figs. 6A, 6E, 6I). Both pCO_2 and $\%N_2O$ were negatively related to pond surface
316 area (Figs. 6A, 6I) and CH_4 was positively related to pond surface area (Fig. 6E). The ponds
317 closer to the city center had lower CH_4 concentrations (Fig. 6F) and higher $\%N_2O$ (Fig. 6J)
318 than the ponds closer to the periphery of the city. $\%N_2O$ values showed a higher dispersion
319 in small ponds than larger ponds and in ponds closer to the city center compared to the
320 periphery of the city. pCO_2 did not show a clear pattern with regards to the city center (Fig.
321 6B). DIN, NO_3^- and NO_2^- concentrations decreased with distance from the city center but not
322 NH_4^+ (Fig. 7). Atmospheric nitrogen dioxide (NO_2) concentration decreased with distance
323 from the city center (Fig. 7E). $\%N_2O$ was positively correlated to the atmospheric NO_2
324 concentration (Fig. 7F). Elevated CH_4 concentrations were observed in ponds with higher
325 macrophyte cover (Fig. 6G). Ponds with high macrophyte cover were located farther away
326 from the city center (Fig. S3A), had larger surface areas (Fig. S3B), and lower residence
327 times (Fig. S3C). Ponds with high macrophyte cover exhibited lower concentrations of DIN
328 and Chl-*a* than ponds with low macrophyte cover (Fig. S3D,E). Ponds with high and low
329 macrophyte cover had no difference in SRP and Ptot concentration (Figs. S3F,G). No
330 significant correlation was observed between Chl-*a* and distance from city center (Fig. S4).

331

332 **3.3. Fluxes of GHGs**

333

334 The mean and median concentrations of the three GHGs in the sampled ponds were
335 consistently higher than their respective equilibrium concentrations (Fig. 3). Consequently,
336 the sampled ponds were sources of GHGs to the atmosphere during all four season,
337 although negative flux values were observed on some rare occasions (Fig. S5). Seasonal
338 variations of the GHG fluxes mirrored those of the respective concentrations because of
339 modest variations of wind speed and computed k_{600}, although higher fluxes were observed
340 during spring characterized by the highest daily wind speeds (Fig. S5A).

341 In terms of GHG emissions expressed in CO_2 equivalents, CO_2 was the dominant
342 GHG emitted, with a median annual emission to the atmosphere of 732 g CO_2 m^{-2} yr^{-1}.
343 Median annual emission of CH_4 and N_2O was 97 and 9 g CO_2-eq m^{-2} yr^{-1} ,respectively. CO_2
344 contributed to 88% of the total CO_2 equivalent emissions, CH_4 contributed to 11%, and N_2O
345 contributed to 1%. The total annual diffusive emissions of CO_2, CH_4, and N_2O amounted to
346 0.8 kT of CO_2-eq for all of the ponds in the city of Brussels (n=158) (Fig. 8).

4. Discussion

4.1. Seasonal variations

Seasonal variations of dissolved CO_2 in lacustrine systems at mid and high latitudes depend on the seasonal alternation between periods of net ecosystem heterotrophy and periods when the aquatic ecosystem evolves to more autotrophic conditions. This seasonal alternation depends on light conditions, with a higher aquatic primary production in spring and summer. Light conditions co-vary with temperature, and warmer conditions coincide seasonally with the sunnier conditions in summer. Allochthonous organic matter inputs from the watershed can also vary seasonally and are usually stronger in fall and winter than spring and summer.

In the sampled ponds of the city of Brussels, the overall negative relation between pCO_2 and $\%O_2$ (Figs. 4A) reflected an alternation between autotrophy-heterotrophy (balance between photosynthesis and community respiration), as also observed in other studies in rivers and lakes (Borges et al., 2015, 2018). This confirmed by the observed relationship between pCO_2 and SRP (Fig. 4F) that may reflect the uptake of nutrients by autotrophic groups leading to the lowering of SRP and pCO_2, and, conversely, high SRP and pCO_2 resulting from the degradation of OM in the water column and sediments (Allesson et al., 2020). The pCO_2 values in the sampled ponds of the city of Brussels were highest in fall and lowest in summer. In fall, the senescence of photosynthetic organisms, induced by a decrease in light intensity and water temperatures, will lead to a large amount of potentially degradable autochthonous OM (Bartosiewicz et al., 2021), which will be respired and lead to higher pCO_2 in fall than in winter and summer. The input in fall of allochthonous OM to ponds is increased with leaf fall from surrounding trees (Sønderup et al., 2016) and with runoff due to higher precipitation . In spring, the occurrence of aquatic primary production in response to the increase of the photoperiod and water temperature, lead to a CO_2 consumption and O_2 production.

In summer, the median (average) pCO_2 was not significantly different compared to other seasons, but there was a higher dispersion of the values that explained the lack of relation between pCO_2 and water temperature and Chl-*a* (Figs. 4B, 4C), unlike CH_4 and

379 $\%N_2O$ that correlated to water temperature (Figs. 4H, 4N). The high dispersion of pCO_2
380 values in summer may be attributed to sampling different stages of phytoplankton
381 development in various ponds during the summer campaign (Fig. S4). Low pCO_2 values
382 were observed in ponds where phytoplankton was blooming and high pCO_2 values were
383 observed in ponds where phytoplankton was senescent. The relation of pCO_2 and Chl-*a*
384 was further complicated by the variable density of macrophyte cover among the different
385 sampled ponds. High macrophyte cover corresponded to low Chl-*a* concentrations, while
386 low macrophyte cover corresponded to higher Chl-*a* levels (Fig. S3D).

387 Low $\%O_2$ values in the water column indicate a generalized net heterotrophy
388 within the sampled ponds including the sediments and therefore also a high
389 methanogenesis, leading to an overall negative relation between CH_4 and $\%O_2$ (Fig. 4G),
390 as also observed in other urban ponds (Audet et al., 2020; Peacock et al., 2021). Since
391 methanogenesis occurs in sediments rich in organic matter, seasonal variations of
392 methanogenesis are very strongly dependent on temperature variations (Zeikus and
393 Winfrey, 1976; Yvon-Durocher et al., 2014; Chen et al., 2021). Consequently, there was also
394 a highly significant positive correlation between CH_4 and water temperature (Fig. 4H). There
395 is a highly significant positive correlation between Ptot and CH_4, as in other urban ponds
396 (Peacock et al., 2019; Rabaey and Cotner, 2022), probably reflecting the delivery of fresh,
397 labile organic matter to sediments enhancing methanogenesis (Grasset et al., 2021; Gruca-
398 Rokosz and Cieśla, 2021 ; Nijman et al., 2022). Ptot was similar in ponds with high and low
399 macrophyte cover (Fig. S3G), indicating Ptot gives a measure of potentially degradable OM
400 from both phytoplankton and macrophytes. Consequently, Ptot was higher in spring and
401 summer (Table S2), when primary production from phytoplankton and macrophytes is
402 highest.

403 N_2O in lakes and ponds results from nitrification and denitrification that show seasonal
404 variations, mainly as a function of DIN availability and O_2 conditions (in particular in thermally
405 stratified systems), as well as water temperature (Myrstener et al., 2016; Palacin-Lizarbe et
406 al., 2018; Mander et al., 2021). Additionally, the yield of N_2O production from both nitrification
407 and denitrification also depends on O_2 levels and water temperature. In the sampled ponds,
408 $\%N_2O$ was higher in fall than summer, as observed by Mander et al. (2021) in artificial
409 wetlands. During fall, high heterotrophic degradation of organic matter and ammonification,
410 combined with lower uptake of NH_4^+ by phytoplankton, resulted in high concentrations of
411 NH_4^+ (Table S2). This led to high N_2O production from nitrification due to higher NH_4^+
412 availability, and the N_2O yield from nitrification was possibly enhanced by low O_2 conditions

(Rosamond et al., 2012; Soued et al., 2016). In spring and summer, the NH_4^+ was assimilated by phytoplankton and there was substrate limitation for N_2O production by nitrification in the water column. The combination of high and low nitrification in fall and spring, respectively explained the observed overall relationship between $\%N_2O$ and NH_4^+ (Fig. 5B). NO_2^- and NO_3^- are, respectively, intermediate and final product of the nitrification, which explained the observed overall relationship between $\%N_2O$ and NO_2^- and NO_3^- (Figs. 5C, 5D) that was statistically more significant than the relation between $\%N_2O$ and NH_4^+. Low O_2 levels will favour N_2O production over NO_2^- production during nitrification (Goreau et al., 1980; Ni et al., 2011), leading to a negative relation between $\%N_2O$ and O_2:DIN, O_2:NO_2^- and O_2:NO_3^- (Figs. 5E, 5G, 5H). While the correlations between N_2O and NH_4^+, NO_3^- and NO_2^- (Figs. 5B, 5C, 5D) in the sampled ponds of the city of Brussels indicate the importance of nitrification in driving the variability of N_2O, denitrification should also have played a role in N_2O dynamics. An indication of this is given by the overall negative relationship between $\%N_2O$ and water temperature (Fig. 4N), as the last step of denitrification is inhibited at low temperatures (Liao et al., 2018; Velthuis and Veraart, 2022), leading to an accumulation of N_2O in the water column during fall and winter. A pattern of higher N_2O levels during wintertime was also observed in boreal lakes and attributed to the effect of temperature on the N_2O yield from denitrification (Kortelainen et al., 2020).

4.2. Spatial variations in GHGs

The levels of CO_2 and CH_4 in lakes vary as a function of lake size (Lapierre and del Giorgio, 2012; Kankaala et al., 2013; Raymond et al., 2013; Holgerson and Raymond, 2016; Casas-Ruiz et al., 2021; Borges et al., 2022; Chiriboga et al. 2024) as well as land cover (Maberly et al., 2013). Combined lake size and land cover determine relative levels of allochthonous organic matter inputs to aquatic systems and the general balance of autotrophy and heterotrophy largely determining CO_2 levels (del Giorgio and Peters, 1994), as well as benthic methanogenesis. The size of the water body will also largely determine the relative importance of soil-water and ground-water inputs of CO_2 and CH_4 (Weyhenmeyer et al., 2015; Olid et al. 2022). The size of the water body will also determine to a larger extent its depth, with smaller systems being in general shallower (Wetzel, 2001). Depth will in turn determine the degree of coupling between sedimentary processes and surface waters, as well as the possibly development of macrophytes. Yet, given the low

number of studies, it has not been investigated if these general patterns established from studies in natural lakes and ponds can be applied to urban ponds. In urban ponds the catchment cover is obviously very different from more natural systems, and there is a very strong atmospheric nitrogen deposition. Inter-lake variations of N_2O have been less investigated than CO_2 and CH_4, although DIN levels and depth are expected to exert a strong influence on N_2O lacustrine levels (Lauerwald et al., 2019; Borges et al., 2022).

The surface area of the sampled ponds was overall low and the range of variation was small (0.1-4.6 ha), so that other properties than pond size might have driven inter-system differences. The analysis of spatial patterns of GHGs in the sampled ponds was complicated by the fact that the smaller systems were located towards the center of city, and the larger ones at the periphery in contact with either cropland to the West and the Sonian forest to the East. Furthermore, the larger systems were characterized by a more important macrophyte cover.

The pCO_2 values in the sampled ponds did not show a significant relation to the distance from the city center or macrophyte cover (Figs. 6B, 6C). However, the pCO_2 values were significantly higher in the smaller systems than the larger ones (Fig. 6A). This agrees with several studies at local, regional or global scales showing a negative relation between pCO_2 and lake surface area (Lapierre and Del Giorgio, 2012; Kankaala et al., 2013; Raymond et al., 2013; Holgerson and Raymond, 2016; Casas-Ruiz et al., 2021). The causes of such relations are related to the overall influence of lake size on inputs from the landscape and lake carbon cycling and have been discussed in detail in several other studies (del Giorgio and Peters, 1994; Sand-Jensen and Staehr, 2007; Borges et al., 2022).

The CH_4 concentration in the sampled ponds was significantly higher in the larger systems than the smaller ones (Fig. 6E). Several studies reported a negative correlation between CH_4 concentration and lake size (surface and/or depth) across spatial scales (local to global) (Borges et al., 2011; Kankaala et al., 2013; Holgerson and Raymond, 2016; Borges et al., 2022; Chiriboga et al. 2024), yet one study reported no relationship (Peacock et al., 2019) and another a positive correlation (Rabaey et al., 2022). The positive relationship between CH_4 concentration and pond size in the ponds of the city of Brussels was probably indirect and reflected another driver. The relationship of CH_4 concentrations in relation to the distance from the city center and to macrophyte cover was statistically more significant than to surface area (Figs. 6E, 6F, 6G). We hypothesize that macrophyte cover was the predominant driver (given the stronger statistical significance) that was itself a function of

distance from the city center. The statistically weak negative relationship between Chl-*a* and CH_4 (Fig. 4J) could reflect the fact that ponds with high macrophyte cover tended to exhibit lower Chl-*a* concentrations (Fig. S3D) but had significantly higher CH_4 concentrations (Fig. 6G).

Submerged macrophytes have a complex impact on CH_4 dynamic in lakes and ponds, as synthesized by Bastviken et al. (2023), with both positive and negative effects on the CH_4 emissions. In the urban ponds of the city of Brussels, the CH_4 concentration was significantly higher in ponds with a high macrophyte cover (Fig. 6G), located in the periphery of the city and closer to the Sonian Forest (Figs. 6F, 6H). In addition to the potential positive impact of macrophytes on CH_4, the Sonian forest likely transfers allochthonous carbon as plant litter promoting CH_4 production compared to other ponds. Litter from trees can induce sediment anoxia (Mehring et al., 2014) enhancing CH_4 production. Yet, this potential additional input of allochthonous organic carbon from the Sonian Forest did not seem to affect the pCO_2 in ponds for which the effect of size seemed more important.

The $\%N_2O$ levels were significantly higher but also more variable in the sampled urban ponds closer to the city center than at the periphery of the city (Figs. 6J, 6L). $\%N_2O$ was strongly correlated to DIN, NO_2^- and NO_3^- concentrations (Fig. 5) that were higher close to the city center (Fig. 7). The higher DIN, NO_2^- and NO_3^- concentrations in the city center could have resulted from higher N deposition as indicated by the pattern of atmospheric NO_2 (Fig. 7E). No correlation was found with macrophyte cover (Fig. 6K), although the presence of macrophytes strongly influences nitrogen cycling in sediments (Barko et al., 1991; Choudhury et al., 2018; Dan et al., 2021; Ni et al., 2022) and could in theory potentially have affected N_2O levels.

4.3. Comparison with other urban and natural ponds

There are only a few equivalent studies of GHG emissions in urban ponds for comparison (Table S3). We restricted the comparison to dissolved GHG concentrations rather than fluxes across the air-water interface. Fluxes measured with floating chambers and computed fluxes from *k* can provide diverging results, so are not necessarily comparable (Duchemin et al., 1999; Guérin et al., 2007; Klaus and Vachon, 2020; Erkkilä et

al., 2018; Perolo et al., 2021). This is possibly related to measurement biases using floating chambers (Belanger and Korzun, 1991; Lorke et al., 2015; Vingiani et al., 2021), although the computation of *k* can be made with different parameterizations derived from several methods (including floating chambers) and that provide different values particularly at high wind speeds. It is unclear which wind parametrization is the most appropriate (Klaus and Vachon, 2020), in particular with regards to effects of size and fetch limitation (Wanninkhof, 1992) which might become very important in small water bodies such as ponds (Holgerson et al., 2017; Jansen et al., 2020). We computed the fluxes from dissolved concentrations of CO_2, CH_4 and N_2O and the gas transfer velocity computed from the parameterization as a function of wind speed of Cole and Caraco (1998). The parametrization of Cole and Caraco (1998) was built from a large compilation of deliberate tracer based estimates of k_{600} in 11 lakes with a wide range of maximum depth (1-109m) and surface area (0.2-487 km^2). The parametrization of Cole and Caraco (1998) parameterization as function of wind speed intrinsically integrates other sources of turbulence (night-time convection due to cooling) and fetch limitation, because it is built on compilation of repeated tracer measurements in several lakes with a wide range of size and depth. Yet, the parameterization of Cole and Caraco (1998) is based on k_{600} data acquired in water bodies with a surface area larger (>4 ha) than the ponds we sampled (0.1-4.6 ha), which admittedly introduces uncertainty in the computation of k_{600}. The computed k_{600} from the sampled ponds with the parametrization of Cole and Caraco (1998) ranged from 2.1 to 2.6 cm h^{-1} in summer and spring, respectively. The overall annual average k_{600} value of 2.3 cm h^{-1} was within the range of k_{600} values (0.9-3.0 cm h^{-1}) reported by Holgerson et al. (2017) in four ponds located in a dense forest, with surface area ~0.02 ha. These four ponds located in a dense forest were smaller than the ponds we sampled (0.1-4.6 ha) that were located in recreational urban parks, hence, less sheltered from wind that in a dense forest. The values of computed k_{600} from the sampled ponds with the parameterization of Cole and Caraco (1998) are also comparable to the values of k_{600} used by Holgerson and Raymond (2016), in a global analysis of CO_2 and CH_4 emissions from ponds, of 1.5 cm h^{-1} for ponds with a surface area <0.1 ha and of 2.0 cm h^{-1} for ponds with a surface are of 0.1-1.0 ha.

The average of CH_4 dissolved concentrations (annual or summer average) in the sampled ponds of Brussels was comparable to the values reported in other urban ponds in the cities of Silkeborg (Denmark, Audet et al., 2020), Uppsala (Sweden, Peacock et al., 2019; Ray et al., 2023), Linkoping (Sweden, Natchimuthu et al., 2014), Minnesota (United States, Rabaey & Cotner, 2022; Ray et al., 2023) and in Salaspils (Latvia, Ray et al., 2023).

The average dissolved CO_2 concentrations in the sampled ponds was also equivalent to the values in the ponds of Silkeborg (average of 4 seasons) (Audet et al., 2020) and possibly lower in summer than the ponds in Uppsala (Peacock et al., 2019).

The extreme variability of CH_4 and CO_2 concentrations seasonally and among ponds indicated by the large values of the standard deviations was observed in all systems (Brussels, Silkeborg, Uppsala, Minnesota and Salaspils) and probably obscured differences among different studies that could have emerged from differences in inputs of allochthonous carbon and nitrogen, despite the differences in the size of the cities, as Brussels (> 1 million inhabitants) is larger than Silkeborg (<50,000 inhabitants) and Uppsala (140,000 inhabitants). The N_2O concentration in the sampled ponds of Brussels was higher than values in the ponds of Silkeborg (average of 4 seasons) (Audet et al., 2020), which might be a consequence of a larger anthropogenic input of nitrogen from atmospheric deposition due to the larger size of the city of Brussels compared to Silkeborg. This was consistent with a higher value of the annual average NH_4^+ concentration in the ponds of Brussels (27±63 µmol L^{-1}) compared to the ponds of Silkeborg (9±14 µmol L^{-1}, Audet et al., 2020). A stronger eutrophication (nitrogen levels) sustaining a higher primary production, might also explain potentially lower CO_2 concentrations in Brussels in summer than in Silkeborg and Uppsala (Table S3).

Concentrations of CO_2 and CH_4 in the sampled ponds of Brussels were >3 times higher than those in natural (non-urban) ponds of similar size reported by Holgerson and Raymond (2016) (Fig. 9). This confirms the emerging idea that artificial inland water bodies (agricultural reservoirs, urban ponds, storm-water retention basins, …) have higher emission rates per m^2 than natural systems (Martinez-Cruz et al., 2017; Grinham et al., 2018; Herrero Ortega et al., 2019; Gorsky et al., 2019; Ollivier et al., 2019; Peacock et al., 2019, 2021; Webb et al., 2019). This seems to result from more important anthropogenic allochthonous inputs of carbon and nitrogen in artificial systems but might also reflect other differences compared to natural systems such as in hydrology (Clifford and Heffernan, 2018).

4.4. Contribution of urban ponds to the GHG budget of the city of Brussels

The CO_2, CH_4 and N_2O air-water fluxes were converted into CO_2 equivalents and the average scaled to total surface area of ponds in the city of Brussels (101 ha). The diffusive

emissions were dominated by CO_2 (88%), followed by CH_4 (11%) and N_2O (1%). The GHG emissions officially accounted from the city of Brussels are overwhelmingly dominated by CO_2 (99.1%) with a very small contribution from N_2O (0.6%) and CH_4 (0.3%). The relative additional contribution of emissions of GHG from ponds to the total urban emissions is different for each of the three GHGs individually (Table S4). The diffusive emissions from ponds correspond to a fraction of the other urban emissions of 1.2% for CH_4, 0.05% for N_2O and 0.03% for CO_2. The total annual GHG diffusive emissions from ponds of 0.8 $kTCO_2eq$ is several orders of magnitude lower and very marginal compared to the three major anthropogenic emissions in the city of Brussels such as energy (1804 $kTCO_2eq\ yr^{-1}$), transport (807 $kTCO_2eq\ yr^{-1}$), and industries (277 $kTCO_2eq\ yr^{-1}$) (Fig. 8). Ebullitive fluxes of CH_4 were measured in four ponds (Leybeek, Pêcheries Royales, Silex, Ten Reuken) during 2021, 2022, and 2023 and ranged from 0.0 to 59.2 mmol $CH_4\ m^{-2}\ d^{-1}$ (unpublished data). Based on an exponential relationship between ebullitive CH_4 and temperature in the 4 sampled ponds (n=39, r^2=0.54, not shown), we scaled the ebullitive CH_4 fluxes to all of ponds in the city of Brussels that summed correspond to an additional GHG emission of 0.2 $kTCO_2$-eq yr^{-1}. When additionally accounting for CH_4 ebullition, the total CH_4 emissions from the urban ponds (0.2 $kTCO_2$-eq yr^{-1}) correspond to 3.7% of the total urban emissions of CH_4.Yet, the total CH_4 emissions (including CH_4 ebullition) from the urban ponds only represented 0.01% of the total GHG emissions of the city of Brussels (2885 $kTCO_2$-eq yr^{-1}). This was consistent with the contribution of CH_4 emissions from streams and ponds of 0.004% to the total GHG emissions from the city of Berlin reported by Herrero Ortega et al (2019). The total annual GHG emissions from urban ponds, (1.0 $kTCO_2$-eq yr^{-1} including CH_4 ebullition) is of the same order of magnitude as smaller GHG emissions such as waste (5.3 $kTCO_2eq\ yr^{-1}$) and agriculture (1.3 $kTCO_2eq\ yr^{-1}$). The total annual GHG emissions from urban ponds was nearly identical than the estimated sink of GHGs from urban green spaces (1.2 $kTCO_2eq\ yr^{-1}$). Urban green spaces (parks and gardens) provide several ecosystem services reviewed by Pataki et al. (2011) including reducing or offsetting GHG emissions. Here, we showed that the emissions of GHGs from ponds almost fully balance the reported GHG sink reported for green spaces in the city of Brussels. As such, GHG emissions from ponds should be accounted among the negative consequences or tradeoffs of implementing green infrastructure, the so-called “ecosystem disservices” according to Pataki et al. (2011).

5. Conclusions

Our study showed that small urban ponds in the public parks of the city of Brussels emit CO_2, CH_4 and N_2O to the atmosphere. The GHG concentrations and emissions in the sampled ponds showed geographical variations that were partly related to differences in morphology (size) but also the position with regards to the city center, and the surrounding landscape for those in the urban periphery (cropland versus forest), as well as the presence of macrophytes. Smaller ponds received larger amounts of allochthonous carbon, either directly as CO_2 or as OM resulting in larger CO_2 production from respiration. Larger ponds emitted more CH_4 contrary to the pattern most commonly described in the literature. This effect was due to the presence of macrophytes and the proximity of the forest in larger ponds at the periphery of the city compared to the smaller ponds located closer to the city center. N_2O levels were higher closer to the city center that we hypothesize resulting from a stronger atmospheric nitrogen deposition based on the patterns of atmospheric NO_2.

Biological processes were the main drivers of GHG production, as showed from relationships of the three GHGs with water temperature, oxygen saturation and nutrients. CH_4 concentrations were positively related to temperature on seasonal time scales due to the dependence of methanogenesis on temperature, as usually observed in aquatic systems (Yvon-Durocher et al., 2014), including urban ponds (Bartosiewicz et al., 2016). On the contrary the N_2O levels were negatively related to temperature possibly reflecting incomplete denitrification at low temperatures, although DIN levels also increased in winter, so it is difficult to separate the impact of both potential drivers.

The GHG emissions from the studied ponds were lower than the other GHG sources from the city such as road transport and building heating. However, urban green spaces are described as important carbon sinks by Pataki et al. (2011), but this sink was offset by emissions from the ponds within these same green spaces in the city of Brussels. CH_4 emissions from inland waters were incorporated in the latest IPCC assessment report (IPCC, 2019) and should now be included in current national inventories. We show that the total CH_4 emissions from the urban ponds (including diffusive and ebullitive components) correspond to a larger fraction of the total respective urban emissions (3.73%) than CO_2 (0.05%) and N_2O (0.03%). The emissions of GHGs from the urban ponds were equivalent to the reported GHG sink reported for green spaces in the city of Brussels.

Audet et al. (2020) proposed to consider the GHG emissions from ponds in the overall GHG assessment of cities to provide a more comprehensive quantification of a city's carbon footprint and fully quantify the ecosystem services provided by urban green spaces. Yet, the

642 total CO_2, N_2O, and CH_4 emissions (including CH_4 ebullition) from the urban ponds only
643 represented 0.04% of the total GHG emissions of the city of Brussels (2885 $kTCO_2$-eq yr^{-1}).

644

645 **Acknowledgements**

646 TB received a funding from the Brussels-Capital Region's institute for the
647 encouragement of scientific research and innovation (Innoviris) as part of the Smartwater
648 project (ref. Innoviris RBC/2020-EPF-6h) and also from the "Fonds pour la formation à la
649 Recherche dans l'Industrie et dans l'Agriculture" (FRIA, Belgium). CH_4 and N_2O analyses
650 were done by Thomas Bousmanne and Ozan Efe. The analysis of total phosphorus was
651 performed at the Institut Meurice, within the Department of Physical Chemistry and Catalysis
652 at Labiris, under the supervision of Vincent Dubois and Grégory Ploeglaerts. AVB is a
653 Research Director at the Fonds National de la Recherche Scientifique.

654

References

Allesson, L., Andersen, T., Dörsch, P., Eiler, A., Wei, J., & Hessen, D. O. (2020). Phosphorus availability promotes bacterial DOC-mineralization, but not cumulative CO2-production. *Frontiers in Microbiology*, *11*, 569879. https://doi.org/10.3389/fmicb.2020.569879

Anderson, M. J. (2006). Distance-based tests for homogeneity of multivariate dispersions. *Biometrics*, *62*(1), 245-253.https://doi.org/10.1111/j.1541-0420.2005.00440.x

Audet, J., Carstensen, M. V., Hoffmann, C. C., Lavaux, L., Thiemer, K., & Davidson, T. A. (2020). Greenhouse gas emissions from urban ponds in Denmark. *Inland Waters*, *10*(3), 373-385 https://doi.org/10.1080/20442041.2020.1730680

Baliña, S., Sanchez, M. L., Izaguirre, I., & del Giorgio, P. A. (2023). Shallow lakes under alternative states differ in the dominant greenhouse gas emission pathways. *Limnology and Oceanography*, *68*(1), 1-13. https://doi.org/10.1002/lno.12243

Barko, J. W., Gunnison, D., & Carpenter, S. R. (1991). Sediment interactions with submersed macrophyte growth and community dynamics. *Aquatic botany*, *41*(1-3), 41-65. https://doi.org/10.1016/0304-3770(91)90038-7

Bartosiewicz, M., Laurion, I., Clayer, F., & Maranger, R. (2016). Heat-wave effects on oxygen, nutrients, and phytoplankton can alter global warming potential of gases emitted from a small shallow lake. *Environmental science & technology*, *50*(12), 6267-6275. https://doi.org/10.1021/acs.est.5b06312

Bartosiewicz, M., Maranger, R., Przytulska, A., & Laurion, I. (2021). Effects of phytoplankton blooms on fluxes and emissions of greenhouse gases in a eutrophic lake. *Water Research*, *196*, 116985. https://doi.org/10.1016/j.watres.2021.116985

Bastviken, D., Treat, C.C., Pangala, S.R., Gauci, V., Enrich-Prast, A., Karlson, M., Gålfalk, M., Romano, M.B., Sawakuchi, H.O., 2023. The importance of plants for methane emission at the ecosystem scale. Aquat Bot 184, 103596. https://doi.org/10.1016/j.aquabot.2022.103596

Bauduin, T., Gypens, N., & Borges, A. V. (2024). Biogeochemical data from urban ponds in Brussels [Data set]. Zenodo. https://doi.org/10.5281/zenodo.10554478

Belanger, T. V., & Korzun, E. A. (1991). Critique of floating-dome technique for estimating reaeration rates. *Journal of Environmental Engineering*, *117*(1), 144-150. https://doi.org/10.1061/(ASCE)0733-9372(1991)117:1(144)

Bettez, N. D., & Groffman, P. M. (2013). Nitrogen deposition in and near an urban ecosystem. *Environmental science & technology*, *47*(11), 6047-6051. https://doi.org/10.1021/es400664b

Bonetti, G., Limpert, K. E., Brodersen, K. E., Trevathan-Tackett, S. M., Carnell, P. E., & Macreadie, P. I. (2022). The combined effect of short-term hydrological and N-fertilization manipulation of wetlands on CO2, CH4, and N2O emissions. *Environmental Pollution*, *294*, 118637. https://doi.org/10.1016/j.envpol.2021.118637

Borges, A. V., Abril, G., Delille, B., Descy, J. P., & Darchambeau, F. (2011). Diffusive methane emissions to the atmosphere from Lake Kivu (Eastern Africa). *Journal of Geophysical Research: Biogeosciences*, *116*(G3). https://doi.org/10.1029/2011JG001673

Borges, A. V., Darchambeau, F., Lambert, T., Bouillon, S., Morana, C., Brouyère, S., Hakoun, V., Jurado, A., Tseng, H.C., Descy, J.P., Roland, F.A.E., (2018). Effects of agricultural land use on fluvial carbon dioxide, methane and nitrous oxide concentrations in a large European river, the Meuse (Belgium). *Science of the Total Environment*, *610*, 342-355. https://doi.org/10.1016/j.scitotenv.2017.08.047

Borges, A. V., Darchambeau, F., Lambert, T., Morana, C., Allen, G. H., Tambwe, E., ... & Bouillon, S. (2019). Variations in dissolved greenhouse gases (CO_2, CH_4, N_2O) in the Congo River network overwhelmingly driven by fluvial-wetland connectivity. *Biogeosciences*, *16*(19), 3801-3834. https://doi.org/10.5194/bg-16-3801-2019

Borges, A. V., Darchambeau, F., Teodoru, C.R., Marwick, T.R., Tamooh, F., Geeraert, N., Omengo, F.O., Guérin, F., Lambert, T., Morana, C., Okuku, E., Bouillon, S., (2015). Globally significant greenhouse-gas emissions from African inland waters. *Nature Geoscience*, *8*(8), 637-642. https://doi.org/10.1038/ngeo2486

Borges, A. V, Deirmendjian, L., Bouillon, S., Okello, W., Lambert, T., Roland, F.A.E., Razanamahandry, V.F., Voarintsoa, N.R.G., Darchambeau, F., Kimirei, I.A., Descy, J., Allen, G.H., Morana, C., (2022). Greenhouse gas emissions from African lakes are no longer a blind spot. *Science Advances*, *8*(25), eabi8716. DOI: 10.1126/sciadv.abi8716

Bowden, W. B., Glime, J. M., et Riis, T., 2017. Macrophytes and Bryophytes, in: Methods in Stream Ecology: Third Edition. Academic Press, pp. 1–494.

Brans, K. I., Engelen, J. M., Souffreau, C., & De Meester, L. (2018). Urban hot-tubs: Local urbanization has profound effects on average and extreme temperatures in ponds. *Landscape and Urban Planning*, *176*, 22-29.https://doi.org/10.1016/j.landurbplan.2018.03.013

Cade, B. S., & Noon, B. R. (2003). A gentle introduction to quantile regression for ecologists. *Frontiers in Ecology and the Environment*, *1*(8), 412-420. https://doi.org/10.1890/1540-9295(2003)001[0412:AGITQR]2.0.CO;2

Casas-Ruiz, J. P., Jakobsson, J., & del Giorgio, P. A. (2021). The role of lake morphometry in modulating surface water carbon concentrations in boreal lakes. *Environmental Research Letters*, *16*(7), 074037. https://doi.org/10.1088/1748-9326/ac0be3

Chen, H., Xu, X., Fang, C., Li, B., & Nie, M. (2021). Differences in the temperature dependence of wetland CO2 and CH4 emissions vary with water table depth. *Nature Climate Change*, *11*(9), 766-771. https://doi.org/10.1038/s41558-021-01108-4

Chiriboga G, S Bouillon & AV Borges (2024) Dissolved greenhouse gas (CO2, CH4, N2O) emissions from highland lakes of the Andes cordillera in Northern Ecuador, Aquatic Sciences, https://doi.org/10.1007/s00027-023-01039-6

Choudhury, M. I., McKie, B. G., Hallin, S., & Ecke, F. (2018). Mixtures of macrophyte growth forms promote nitrogen cycling in wetlands. *Science of the Total Environment*, *635*, 1436-1443. https://doi.org/10.1016/j.scitotenv.2018.04.193

Clifford, C. C., & Heffernan, J. B. (2018). Artificial aquatic ecosystems. *Water*, *10*(8), 1096. https://doi.org/10.3390/w10081096

Codispoti, L. A., & Christensen, J. P. (1985). Nitrification, denitrification and nitrous oxide cycling in the eastern tropical South Pacific Ocean. *Marine chemistry*, *16*(4), 277-300. https://doi.org/10.1016/0304-4203(85)90051-9

Cole, J. J., & Caraco, N. F. (2001). Carbon in catchments: connecting terrestrial carbon losses with aquatic metabolism. *Marine and Freshwater Research*, *52*(1), 101-110. https://doi.org/10.1071/MF00084

Cole, J. J., & Caraco, N. F. (1998). Atmospheric exchange of carbon dioxide in a low-wind oligotrophic lake measured by the addition of SF6. *Limnology and Oceanography*, *43*(4), 647-656. https://doi.org/10.4319/lo.1998.43.4.0647

Conrad, R. (2020). Methane production in soil environments—anaerobic biogeochemistry and microbial life between flooding and desiccation. *Microorganisms*, *8*(6), 881. https://doi.org/10.3390/microorganisms8060881

Dan, Z., Chuan, W., Qiaohong, Z., & Xingzhong, Y. (2021). Sediments nitrogen cycling influenced by submerged macrophytes growing in winter. *Water Science and Technology*, *83*(7), 1728-1738. https://doi.org/10.2166/wst.2021.081

Davidson, T. A., Audet, J., Svenning, J. C., Lauridsen, T. L., Søndergaard, M., Landkildehus, F., ... & Jeppesen, E. (2015). Eutrophication effects on greenhouse gas fluxes from shallow-lake mesocosms override those of climate warming. *Global Change Biology*, *21*(12), 4449-4463. https://doi.org/10.1111/gcb.13062Davidson, T. A., Sayer, C. D., Jeppesen, E., Søndergaard, M., Lauridsen, T. L., Johansson, L. S., ... & Graeber, D. (2023). Bimodality and alternative equilibria do not help explain long-term patterns in shallow lake chlorophyll-a. *Nature communications*, *14*(1), 398. https://doi.org/10.1038/s41467-023-36043-9

De Backer, S., Van Onsem, S., & Triest, L. (2010). Influence of submerged vegetation and fish abundance on water clarity in peri-urban eutrophic ponds. *Hydrobiologia*, *656*, 255-267. https://doi.org/10.1007/s10750-010-0444-z

Decina, S. M., Hutyra, L. R., & Templer, P. H. (2020). Hotspots of nitrogen deposition in the world's urban areas: a global data synthesis. *Frontiers in Ecology and the Environment*, *18*(2), 92-100. https://doi.org/10.1002/fee.2143

Del Giorgio, P. A., Cole, J. J., Caraco, N. F., & Peters, R. H. (1999). Linking planktonic biomass and metabolism to net gas fluxes in northern temperate lakes. *Ecology*, *80*(4), 1422-1431. https://doi.org/10.1890/0012-9658(1999)080[1422:LPBAMT]2.0.CO;2

Del Giorgio, P. A., & Peters, R. H. (1994). Patterns in planktonic P: R ratios in lakes: influence of lake trophy and dissolved organic carbon. *Limnology and oceanography*, *39*(4), 772-787. https://doi.org/10.4319/lo.1994.39.4.0772

DelSontro, T., Beaulieu, J. J., & Downing, J. A. (2018). Greenhouse gas emissions from lakes and impoundments: Upscaling in the face of global change. *Limnology and Oceanography Letters*, *3*(3), 64-75. https://doi.org/10.1002/lol2.10073

Descy, J. P., Leprieur, F., Pirlot, S., Leporcq, B., Van Wichelen, J., Peretyatko, A., ... & Wilmotte, A. (2016). Identifying the factors determining blooms of cyanobacteria in a set of shallow lakes. *Ecological Informatics*, *34*, 129-138. https://doi.org/10.1016/j.ecoinf.2016.05.003

Desrosiers, K., DelSontro, T., & del Giorgio, P. A. (2022). Disproportionate Contribution of Vegetated Habitats to the CH 4 and CO 2 Budgets of a Boreal Lake. *Ecosystems*, 1-20.. https://doi.org/10.1007/s10021-021-00730-9

Dickson, A.G.; Sabine, C.L. and Christian, J.R. (eds) (2007) Guide to best practices for ocean CO2 measurement. Sidney, British Columbia, North Pacific Marine Science Organization, 191pp. (PICES Special Publication 3; IOCCP Report 8). https://doi.org/10.25607/OBP-1342

Drake, T. W., Raymond, P. A., & Spencer, R. G. (2018). Terrestrial carbon inputs to inland waters: A current synthesis of estimates and uncertainty. *Limnology and Oceanography Letters*, *3*(3), 132-142. https://doi.org/10.1002/lol2.10055

Duchemin, E., Lucotte, M., & Canuel, R. (1999). Comparison of static chamber and thin boundary layer equation methods for measuring greenhouse gas emissions from large water bodies §. *Environmental Science & Technology*, *33*(2), 350-357. https://doi.org/10.1021/es9800840

Dutton, Geoffrey; James Elkins II, Bradley Hall, and NOAA ESRL (2017): Earth System Research Laboratory Halocarbons and Other Atmospheric Trace Gases Chromatograph for Atmospheric Trace Species (CATS) Measurements, Version 1. [Database : atmospheric nitrous oxide N2O]. NOAA National Centers for Environmental Information. [2023-06-21]. https://doi.org/https://doi.org/10.7289/V5X0659V

Erkkilä, K. M., Ojala, A., Bastviken, D., Biermann, T., Heiskanen, J. J., Lindroth, A., ... & Mammarella, I. (2018). Methane and carbon dioxide fluxes over a lake: comparison between eddy covariance, floating chambers and boundary layer method. *Biogeosciences*, *15*(2), 429-445. https://doi.org/10.5194/bg-15-429-2018

Gasith, A., & Hosier, A. D. (1976). Airborne litterfall as a source of organic matter in lakes 1. *Limnology and Oceanography*, *21*(2), 253-258. https://doi.org/10.4319/lo.1976.21.2.0253

Goreau, T. J., Kaplan, W. A., Wofsy, S. C., McElroy, M. B., Valois, F. W., & Watson, S. W. (1980). Production of NO2-and N2O by nitrifying bacteria at reduced concentrations of oxygen. *Applied and environmental microbiology*, *40*(3), 526-532. https://doi.org/10.1128/aem.40.3.526-532.1980

Gorsky, A. L., Racanelli, G. A., Belvin, A. C., & Chambers, R. M. (2019). Greenhouse gas flux from stormwater ponds in southeastern Virginia (USA). *Anthropocene*, *28*, 100218. https://doi.org/10.1016/j.ancene.2019.100218

Grasset, C., Abril, G., Mendonça, R., Roland, F., & Sobek, S. (2019). The transformation of macrophyte-derived organic matter to methane relates to plant water and nutrient contents. *Limnology and Oceanography*, *64*(4), 1737-1749. https://doi.org/10.1002/lno.11148

Grasset, C., Moras, S., Isidorova, A., Couture, R. M., Linkhorst, A., & Sobek, S. (2021). An empirical model to predict methane production in inland water sediment from particular organic matter supply and reactivity. *Limnology and Oceanography*, *66*(10), 3643-3655.. https://doi.org/10.1002/lno.11905

Grasset, C., Sobek, S., Scharnweber, K., Moras, S., Villwock, H., Andersson, S., Hiller, C., Nydahl, A.C., Chaguaceda, F., Colom, W., Tranvik, L.J., 2020. The CO2-equivalent balance of freshwater ecosystems is non-linearly related to productivity. *Global Change Biology*, *26*(10), 5705-5715. https://doi.org/10.1111/gcb.15284

Grasshoff, K., & Johannsen, H. (1972). A new sensitive and direct method for the automatic determination of ammonia in sea water. *ICES Journal of Marine Science*, *34*(3), 516-521. https://doi.org/10.1093/icesjms/34.3.516

Grasshoff, K., Kremling, K., & Ehrhardt, M. (Eds.). (2009). *Methods of seawater analysis :* Determination of nitrite. John Wiley & Sons

Grinham, A., Albert, S., Deering, N., Dunbabin, M., Bastviken, D., Sherman, B., Lovelock, C.E., Evans, C.D., (2018). The importance of small artificial water bodies as sources of methane emissions in Queensland, Australia. *Hydrology and Earth System Sciences*, *22*(10), 5281-5298. https://doi.org/10.5194/hess-22-5281-2018

Gruca-Rokosz, R., & Cieśla, M. (2021). Sediment methane production within eutrophic reservoirs: The importance of sedimenting organic matter. *Science of The Total Environment*, *799*, 149219. https://doi.org/10.1016/j.scitotenv.2021.149219

Guérin, F., Abril, G., Serça, D., Delon, C., Richard, S., Delmas, R., Tremblay, A., Varfalvy, L., (2007). Gas transfer velocities of CO2 and CH4 in a tropical reservoir and its river downstream. *Journal of Marine Systems*, *66*(1-4), 161-172.https://doi.org/10.1016/j.jmarsys.2006.03.019

Hanson, P. C., Carpenter, S. R., Cardille, J. A., Coe, M. T., & Winslow, L. A. (2007). Small lakes dominate a random sample of regional lake characteristics. *Freshwater Biology*, *52*(5), 814-822. https://doi.org/10.1111/j.1365-2427.2007.01730.x

Harpenslager, S.F., Thiemer, K., Levertz, C., Misteli, B., Sebola, K.M., Schneider, S.C., Hilt, S. and Köhler, J. (2022) Short-term effects of macrophyte removal on emission of CO2 and CH4 in shallow lakes. Aquatic Botany 182, 103555. https://doi.org/10.1016/j.aquabot.2022.103555

Herrero Ortega, S., Romero González-Quijano, C., Casper, P., Singer, G. A., & Gessner, M. O. (2019). Methane emissions from contrasting urban freshwaters: Rates, drivers, and a whole-city footprint. *Global change biology*, *25*(12), 4234-4243. https://doi.org/10.1111/gcb.14799

Holgerson, M., Raymond, P. Large contribution to inland water CO_2 and CH_4 emissions from very small ponds. *Nature Geosci* **9**, 222–226 (2016). https://doi.org/10.1038/ngeo2654

Holgerson, M. A., Farr, E. R., & Raymond, P. A. (2017). Gas transfer velocities in small forested ponds. *Journal of Geophysical Research: Biogeosciences*, *122*(5), 1011-1021. https://doi.org/10.1002/2016JG003734

IPCC : Intergovernmental Panel on Climate Change. 2019. 2019 Refinement to the 2006 IPCC guidelines for national greenhouse gas inventories: wetlands. Switzerland: IPCC.

Jansen, J., Thornton, B. F., Cortés, A., Snöälv, J., Wik, M., MacIntyre, S., & Crill, P. M. (2020). Drivers of diffusive CH 4 emissions from shallow subarctic lakes on daily to multi-year timescales. *Biogeosciences*, *17*(7), 1911-1932. https://doi.org/10.5194/bg-17-1911-2020

Kankaala, P., Huotari, J., Tulonen, T., & Ojala, A. (2013). Lake-size dependent physical forcing drives carbon dioxide and methane effluxes from lakes in a boreal landscape. *Limnology and Oceanography*, *58*(6), 1915-1930. https://doi.org/10.4319/lo.2013.58.6.1915

Keller, M., and Stallard, R. F. (1994), Methane emission by bubbling from Gatun Lake, Panama, *J. Geophys. Res.*, 99(D4), 8307–8319, https://doi.org/10.1029/92JD02170

Klaus, M., & Vachon, D. (2020). Challenges of predicting gas transfer velocity from wind measurements over global lakes. *Aquatic Sciences*, *82*(3), 53. https://doi.org/10.1007/s00027-020-00729-9

Koenker, R. (2005). *Quantile regression* (Vol. 38). Cambridge university press. https://doi.org/10.1017/CBO9780511754098

Koroleff, J. (1983). Determination of total phosphorus by alkaline persulphate oxidation. *Methods of Seawater Analysis. Verlag Chemie, Wienheim*, 136-138.

Kortelainen, P., Larmola, T., Rantakari, M., Juutinen, S., Alm, J., & Martikainen, P. J. (2020). Lakes as nitrous oxide sources in the boreal landscape. *Global Change Biology*, *26*(3), 1432-1445. https://doi.org/10.1111/gcb.14928

Lapierre, J. F., & del Giorgio, P. A. (2012). Geographical and environmental drivers of regional differences in the lake pCO2 versus DOC relationship across northern landscapes. *Journal of Geophysical Research: Biogeosciences*, *117*(G3). https://doi.org/10.1029/2012JG001945

Lauerwald, R., Regnier, P., Figueiredo, V., Enrich-Prast, A., Bastviken, D., Lehner, B., ... & Raymond, P. (2019). Natural lakes are a minor global source of N2O to the atmosphere. *Global Biogeochemical Cycles*, *33*(12), 1564-1581. https://doi.org/10.1029/2019GB006261

Liao, R., Miao, Y., Li, J., Li, Yan, Wang, Z., Du, J., Li, Yueming, Li, A., Shen, H., (2018). Temperature dependence of denitrification microbial communities and functional genes in an expanded granular sludge bed reactor treating nitrate-rich wastewater. *RSC advances*, *8*(73), 42087-42094. https://doi.org/10.1039/c8ra08256a

Lorke, A., Bodmer, P., Noss, C., Alshboul, Z., Koschorreck, M., Somlai-Haase, C., Bastviken, D., Flury, S., McGinnis, D.F., Maeck, A., Müller, D., Premke, K., (2015). drifting versus anchored flux chambers for measuring greenhouse gas emissions from running waters. *Biogeosciences*, *12*(23), 7013-7024. https://doi.org/10.5194/bg-12-7013-2015

Maberly, S. C., Barker, P. A., Stott, A. W., & De Ville, M. M. (2013). Catchment productivity controls CO2 emissions from lakes. *Nature Climate Change*, *3*(4), 391-394. https://doi.org/10.1038/nclimate1748

Mander, Ü., Tournebize, J., Espenberg, M., Chaumont, C., Torga, R., Garnier, J., ... & Soosaar, K. (2021). High denitrification potential but low nitrous oxide emission in a constructed wetland treating nitrate-polluted agricultural run-off. *Science of the Total Environment*, *779*, 146614. https://doi.org/10.1016/j.scitotenv.2021.146614

Martinez-Cruz, K., Gonzalez-Valencia, R., Sepulveda-Jauregui, A., Plascencia-Hernandez, F., Belmonte-Izquierdo, Y., & Thalasso, F. (2017). Methane emission from aquatic ecosystems of Mexico City. *Aquatic Sciences*, *79*, 159-169. https://doi.org/10.1007/s00027-016-0487-y

McClure, R. P., Lofton, M. E., Chen, S., Krueger, K. M., Little, J. C., & Carey, C. C. (2020). The magnitude and drivers of methane ebullition and diffusion vary on a longitudinal gradient in a small freshwater reservoir. *Journal of Geophysical Research: Biogeosciences*, *125*(3), e2019JG005205. https://doi.org/10.1029/2019JG005205

McCrackin, M. L., & Elser, J. J. (2011). Greenhouse gas dynamics in lakes receiving atmospheric nitrogen deposition. *Global Biogeochemical Cycles*, *25*(4). https://doi.org/10.1029/2010GB003897

Mehring, A. S., Kuehn, K. A., Tant, C. J., Pringle, C. M., Lowrance, R. R., & Vellidis, G. (2014). Contribution of surface leaf-litter breakdown and forest composition to benthic oxygen demand and ecosystem respiration in a South Georgia blackwater river. *Freshwater Science*, *33*(2), 377-389. https://doi.org/10.1086/675507

Mengis, M., Gächter, R., & Wehrli, B. (1997). Sources and sinks of nitrous oxide (N 2 O) in deep lakes. *Biogeochemistry*, *38*, 281-301. https://doi.org/10.1023/A:1005814020322

Myrhe, G., Shindell, D., Bréon, F.-M., Collins, W., Al., E., 2013. Anthropogenic and natural radiative forcing. Climate Change 2013 the Physical Science Basis: Working Group I Contribution to the Fifth Assessment Report of the Intergovernmental Panel on Climate Change. Chapter 8 : Anthropogenic and Natural Radiative Forcing 9781107057, 659–740. https://doi.org/10.1017/CBO9781107415324.018

Myrstener, M., Jonsson, A., & Bergström, A. K. (2016). The effects of temperature and resource availability on denitrification and relative N2O production in boreal lake sediments. *Journal of Environmental Sciences*, *47*, 82-90. https://doi.org/10.1016/j.jes.2016.03.003

Natchimuthu, S., Panneer Selvam, B., & Bastviken, D. (2014). Influence of weather variables on methane and carbon dioxide flux from a shallow pond. *Biogeochemistry*, *119*, 403-413. https://doi.org/10.1007/s10533-014-9976-z

Ni, B. J., Ruscalleda, M., Pellicer-Nacher, C., & Smets, B. F. (2011). Modeling nitrous oxide production during biological nitrogen removal via nitrification and denitrification: extensions to the general ASM models. *Environmental science & technology*, *45*(18), 7768-7776. https://doi.org/10.1021/es404125v

Ni, M., Liang, X., Hou, L., Li, W., & He, C. (2022). Submerged macrophytes regulate diurnal nitrous oxide emissions from a shallow eutrophic lake: A case study of Lake Wuliangsuhai in the temperate arid region of China. *Science of The Total Environment*, *811*, 152451. https://doi.org/10.1016/j.scitotenv.2021.152451

Nijman, T. P., Lemmens, M., Lurling, M., Kosten, S., Welte, C., & Veraart, A. J. (2022). Phosphorus control and dredging decrease methane emissions from shallow lakes. *Science of the Total Environment*, *847*, 157584. https://doi.org/10.1016/j.scitotenv.2022.157584

Oksanen, r J., Simpson, G.L., Blanchet, F.G., Solymos, P., Stevens, M.H.H., Szoecs, E., Wagner, H., Barbour, M., Bedward, M., Bolker, B., Borcard, D., Carvalho, G., Chirico, M., Durand, S., Beatriz, H., Evangelista, A., Friendly, M., Hannigan, G., Hill, M.O., Lahti, L., Mcglinn, D., Ribeiro, E., Smith, T., Stier, A., Ter, C.J.F., Weedon, J., (2013). Package 'vegan'. *Community ecology package, version*, *2*(9), 1-295.https://cran.r-project.org/web/packages/vegan/index.html

Olid C, V Rodellas, G Rocher-Ros, J Garcia-Orellana, M Diego-Feliu, A Alorda-Kleinglass, D Bastviken & J Karlsson, Groundwater discharge as a driver of methane emissions from Arctic lakes, NATURE COMMUNICATIONS, (2022) 13:3667, https://doi.org/10.1038/s41467-022-31219-1

Ollivier, Q. R., Maher, D. T., Pitfield, C., & Macreadie, P. I. (2019). Punching above their weight: Large release of greenhouse gases from small agricultural dams. *Global change biology*, *25*(2), 721-732. https://doi.org/10.1111/gcb.14477

Palacin-Lizarbe, C., Camarero, L., & Catalan, J. (2018). Denitrification Temperature Dependence in Remote, Cold, and N-Poor Lake Sediments. *Water Resources Research*, *54*(2), 1161-1173. https://doi.org/10.1002/2017WR021680

Pataki, D.E., Carreiro, M.M., Cherrier, J., Grulke, N.E., Jennings, V., Pincetl, S., Pouyat, R. V., Whitlow, T.H., Zipperer, W.C., (2011). Coupling biogeochemical cycles in urban environments: ecosystem services, green solutions, and misconceptions. *Frontiers in Ecology and the Environment*, *9*(1), 27-36. https://doi.org/10.1890/090220

Peacock, M., Audet, J., Bastviken, D., Cook, S., Evans, C.D., Grinham, A., Holgerson, M.A., Högbom, L., Pickard, A.E., Zieliński, P., Futter, M.N., (2021). Small artificial waterbodies are widespread and persistent emitters of methane and carbon dioxide. *Global Change Biology*, *27*(20), 5109-5123. https://doi.org/10.1111/gcb.15762

Peacock, M., Audet, J., Jordan, S., Smeds, J., & Wallin, M. B. (2019). Greenhouse gas emissions from urban ponds are driven by nutrient status and hydrology. *Ecosphere*, *10*(3), e02643. https://doi.org/10.1002/ecs2.2643

Peretyatko, A., Symoens, J. J., & Triest, L. (2007). Impact of macrophytes on phytoplankton in eutrophic peri-urban ponds, implications for pond management and restoration. *Belgian Journal of Botany*, 83-99. https://www.jstor.org/stable/20794626

Peretyatko, A., Teissier, S., De Backer, S., & Triest, L. (2012). Classification trees as a tool for predicting cyanobacterial blooms. *Hydrobiologia*, *689*, 131-146. https://doi.org/10.1007/s10750-011-0803-4

Peretyatko, A., Teissier, S., De Backer, S., & Triest, L. (2010). Restoration potential of biomanipulation for eutrophic peri-urban ponds: the role of zooplankton size and submerged macrophyte cover. *Pond Conservation in Europe*, 281-291. https://doi.org/10.1007/s10750-009-9888-4

Perolo, P., Fernández Castro, B., Escoffier, N., Lambert, T., Bouffard, D., & Perga, M. E. (2021). Accounting for surface waves improves gas flux estimation at high wind speed in a large lake. *Earth System Dynamics*, *12*(4), 1169-1189. https://doi.org/10.5194/esd-12-1169-2021

R Core Team, 2022. R: A Language and Environment for Statistical Computing. https://www.r-project.org/

Rabaey, J., & Cotner, J. (2022). Pond greenhouse gas emissions controlled by duckweed coverage. *Frontiers in Environmental Science*, *10*, 889289. https://doi.org/10.3389/fenvs.2022.889289

Ray, N.E., Holgerson, M.A., Andersen, M.R., Bortolotti, L.E., Futter, M., Kokor, I., Law, A., Mcdonald, C., Mesman, J.P., Peacock, M., (2023). Spatial and temporal variability in summertime dissolved carbon dioxide and methane in temperate ponds and shallow lakes. *Limnology and Oceanography*. https://doi.org/10.1002/lno.12362

Raymond, P.A., Hartmann, J., Lauerwald, R., Sobek, S., McDonald, C., Hoover, M., Butman, D., Striegl, R., Mayorga, E., Humborg, C., Kortelainen, P., Dürr, H., Meybeck, M., Ciais, P., Guth, P., (2013). Global carbon dioxide emissions from inland waters. *Nature*, *503*(7476), 355-359. https://doi.org/10.1038/nature12760

Rosamond, M. S., Thuss, S. J., & Schiff, S. L. (2012). Dependence of riverine nitrous oxide emissions on dissolved oxygen levels. *Nature Geoscience*, *5*(10), 715-718. https://doi.org/10.1038/ngeo1556

Rosentreter, J.A., Borges, A. V., Deemer, B.R., Holgerson, M.A., Liu, S., Song, C., Melack, J., Raymond, P.A., Duarte, C.M., Allen, G.H., Olefeldt, D., Poulter, B., Battin, T.I., Eyre, B.D., (2021). Half of global methane emissions come from highly variable aquatic ecosystem sources. *Nature Geoscience*, *14*(4), 225-230. https://doi.org/10.1038/s41561-021-00715-2

Sand-Jensen, K., & Staehr, P. A. (2007). Scaling of pelagic metabolism to size, trophy and forest cover in small Danish lakes. *Ecosystems*, *10*, 128-142. https://doi.org/10.1007/s10021-006-9001-z

Singh, S. N., Kulshreshtha, K., & Agnihotri, S. (2000). Seasonal dynamics of methane emission from wetlands. *Chemosphere-Global Change Science*, *2*(1), 39-46. https://doi.org/10.1016/S1465-9972(99)00046-X

Sønderup, M. J., Egemose, S., Hansen, A. S., Grudinina, A., Madsen, M. H., & Flindt, M. R. (2016). Factors affecting retention of nutrients and organic matter in stormwater ponds. *Ecohydrology*, *9*(5), 796-806. https://doi.org/10.1002/eco.1683

Soued, C., Del Giorgio, P. A., & Maranger, R. (2016). Nitrous oxide sinks and emissions in boreal aquatic networks in Québec. *Nature Geoscience*, *9*(2), 116-120. https://doi.org/10.1038/ngeo2611

U.S. EPA. 2007. "Method 3015A (SW-846): Microwave Assisted Acid Digestion of Aqueous Samples and Extracts," Revision 1. Washington, DC *https://www.epa.gov/esam/epa-method-3015a-microwave-assisted-acid-digestion-aqueous-samples-and-extracts*

U.S. EPA. 1994. "Method 200.7: Determination of Metals and Trace Elements in Water and Wastes by Inductively Coupled Plasma-Atomic Emission Spectrometry," Revision 4.4. Cincinnati, OH. https://www.epa.gov/esam/method-2007-determination-metals-and-trace-elements-water-and-wastes-inductively-coupled

Vachon, D., Langenegger, T., Donis, D., Beaubien, S. E., & McGinnis, D. F. (2020). Methane emission offsets carbon dioxide uptake in a small productive lake. *Limnology and Oceanography Letters*, *5*(6), 384-392. https://doi.org/10.1002/lol2.10161

van Bergen, T.J.H.M., Barros, N., Mendonça, R., Aben, R.C.H., Althuizen, I.H.J., Huszar, V., Lamers, L.P.M., Lürling, M., Roland, F., Kosten, S., (2019). Seasonal and diel variation in greenhouse gas emissions from an urban pond and its major drivers. *Limnology and Oceanography*, *64*(5), 2129-2139. https://doi.org/10.1002/lno.11173

van Nes, E. H., Scheffer, M., van den Berg, M. S., & Coops, H. (2002). Dominance of charophytes in eutrophic shallow lakes—when should we expect it to be an alternative stable state?. *Aquatic Botany*, *72*(3-4), 275-296. https://doi.org/10.1016/S0304-3770(01)00206-6

Velthuis, M., & Veraart, A. J. (2022). Temperature Sensitivity of Freshwater Denitrification and N2O Emission—A Meta-Analysis. *Global Biogeochemical Cycles*, *36*(6), e2022GB007339. https://doi.org/10.1029/2022GB007339

Vingiani, F., Durighetto, N., Klaus, M., Schelker, J., Labasque, T., & Botter, G. (2021). Evaluating stream CO 2 outgassing via drifting and anchored flux chambers in a controlled flume experiment. *Biogeosciences*, *18*(3), 1223-1240. https://doi.org/10.5194/bg-18-1223-2021

Wanninkhof, R. (1992). Relationship between gas exchange and wind speed over the ocean. *J. Geophys. Res.*, *97*, 7373-7381. https://doi.org/10.1029/92JC00188

Webb, J. R., Leavitt, P. R., Simpson, G. L., Baulch, H. M., Haig, H. A., Hodder, K. R., & Finlay, K. (2019). Regulation of carbon dioxide and methane in small agricultural reservoirs: optimizing potential for greenhouse gas uptake. *Biogeosciences*, *16*(21), 4211-4227. https://doi.org/10.5194/bg-16-4211-2019

Wetzel, R. G. (2001). *Limnology: lake and river ecosystems*. gulf professional publishing.

1005 Weyhenmeyer, G. A., Kosten, S., Wallin, M. B., Tranvik, L. J., Jeppesen, E., & Roland, F. (2015). Significant
1006 fraction of CO2 emissions from boreal lakes derived from hydrologic inorganic carbon inputs. *Nature*
1007 *Geoscience*, *8*(12), 933-936. https://doi.org/10.1038/ngeo2582

1008 Yentsch, C. S., & Menzel, D. W. (1963, July). A method for the determination of phytoplankton chlorophyll and
1009 phaeophytin by fluorescence. In *Deep Sea Research and Oceanographic Abstracts* (Vol. 10, No. 3,
1010 pp. 221-231). Elsevier. https://doi.org/10.1016/0011-7471(63)90358-9

1011 Yvon-Durocher, G., Allen, A.P., Bastviken, D., Conrad, R., Gudasz, C., St-Pierre, A., Thanh-Duc, N., Del
1012 Giorgio, P.A., (2014). Methane fluxes show consistent temperature dependence across microbial to
1013 ecosystem scales. *Nature*, *507*(7493), 488-491.https://doi.org/10.1038/nature13164

1014 Zeikus, J. G., & Winfrey, M. (1976). Temperature limitation of methanogenesis in aquatic sediments. *Applied*
1015 *and environmental microbiology*, *31*(1), 99-107. https://doi.org/10.1128/aem.31.1.99-107.1976

1016

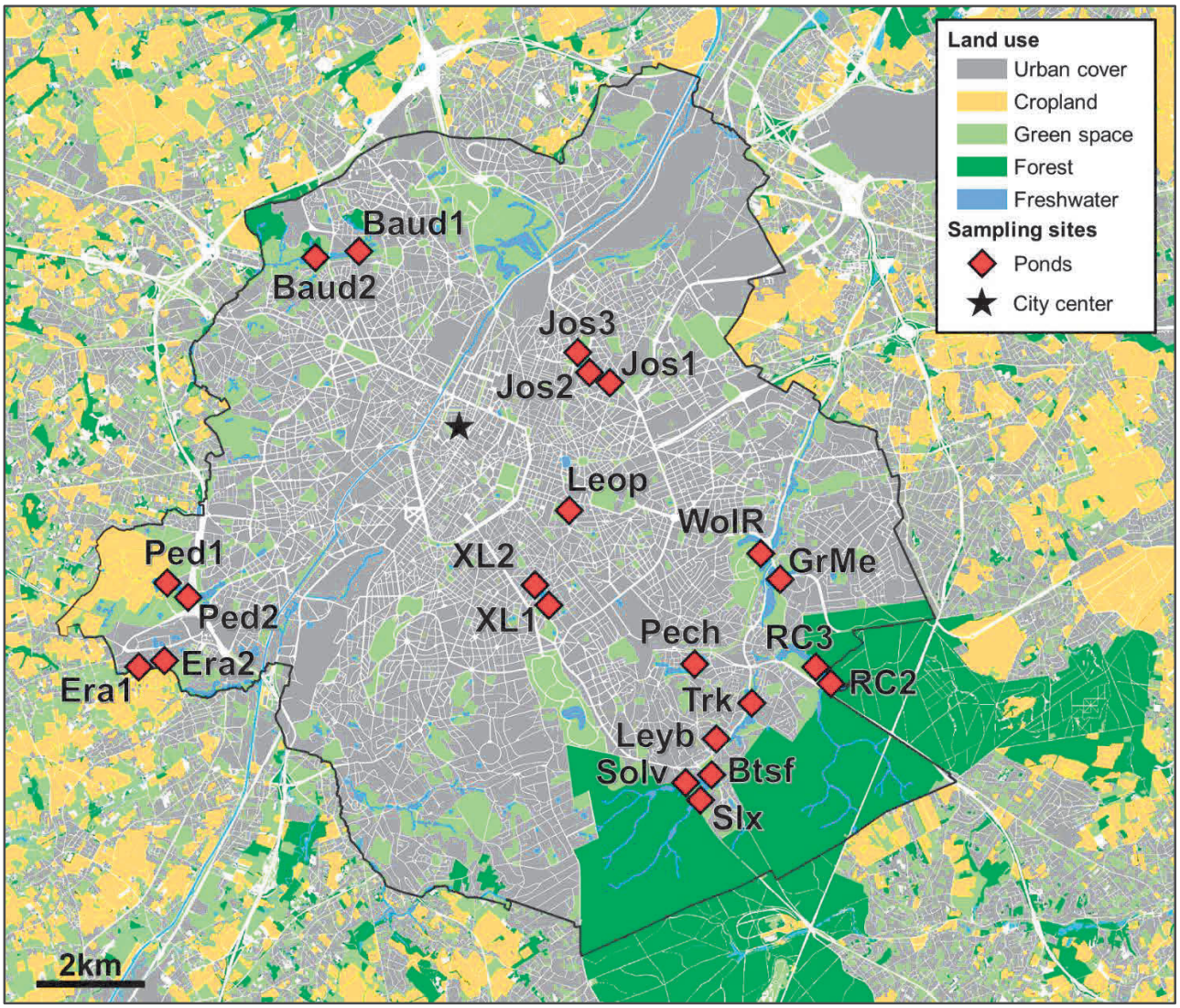

Figure 1 : Map of the metropolitan area of the region of Brussels delineated by the black line and surrounding region of Flanders in Belgium showing land cover and sampling locations in ponds (red diamonds). The star corresponds to the center of the city (50.8504°N, 4.3487°E). The acronyms correspond to the official names of the ponds of Bruxelles Environnement, the regional water management agency (Baud 1 : Etang Parc Roi Baudouin Phase I ; Baud2 : Etang Parc Roi Baudouin Phase II ; Btsf : Etang de Boitsfort ; Era 1 : Etang Erasme amont ; Era 2 : Etang Erasme aval ; GrMe : Grand étang Mellaerts ; Jos1 : Parc Josaphat - Etang aux canards ; Jos2 : Parc Josaphat – Etang aux pigeons ; Jos3 : Parc Josaphat – Etang de la laiterie ; Leop : Etang parc Leopold ; Leyb : Etang du Leybeek ; Pech : Etang Pêcheries Royales ; Ped1 : Etang de la Pède Grand Etang ; Ped2 : Etang de la Pède ; RC2 : Grand étang des Clabots (Etang 2) ; RC3 : Etang du moulin (Etang 3) ; Slx : Etang du Silex ; Solv : Grand étang – Parc Tournay Solvay ; Trk : Etang Parc Ten Reuken ; WolR : Etang rond – Parc de Woluwe ; XL1 : Etang d'Ixelles Nord ; XL2 : Etang d'Ixelles Sud). The shape of each pond and connection to the hydrological network is shown in Figure S1.

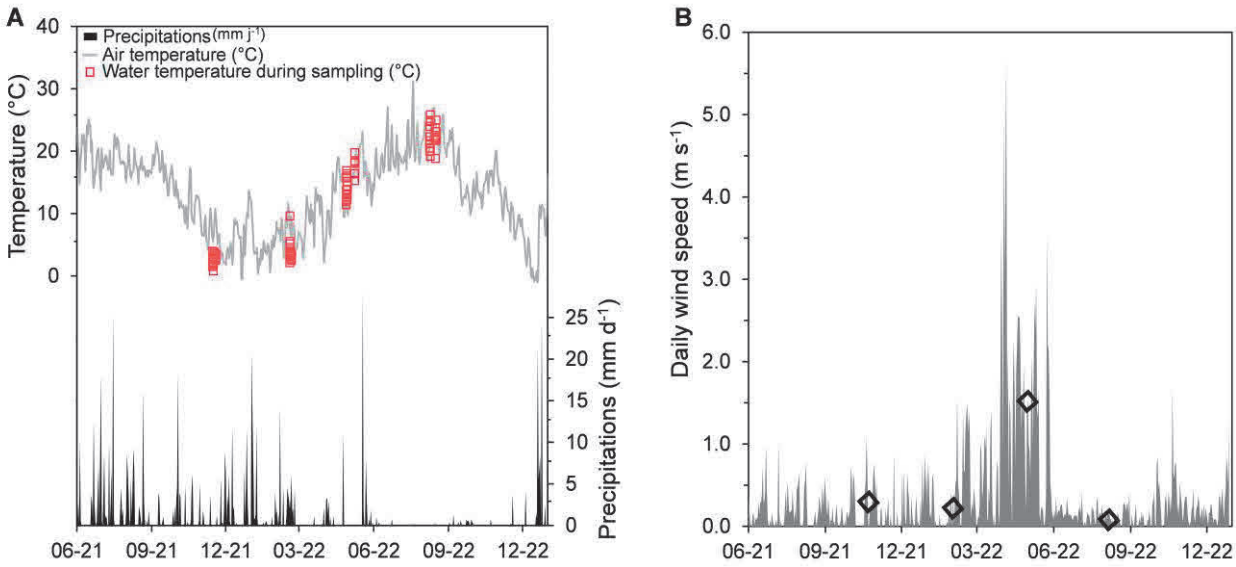

Figure 2 : Daily mean air temperature (light grey line), daily precipitation (black line) (A) and daily wind speed (dark grey, right) (B). The empty red squares on (A) indicate the in-situ water temperature during sampling and the empty black diamonds on (B) indicate the average wind during each sampling period. Meteorological data were obtained from crowdsourcing platform of the Royal Belgian Meteorological Institute (wow.meteo.be) at the Brussels–Woluwe Saint Lambert station (50.8408 °N, 4.4234 °E).

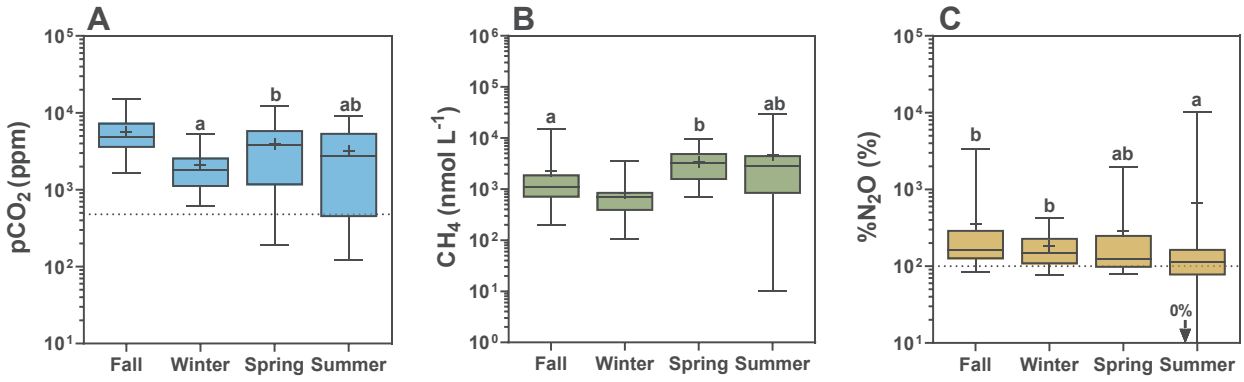

Figure 3 : Seasonal variations of partial pressure of CO_2 (pCO_2 in ppm) (A); dissolved CH_4 concentration (CH_4 in nmol L^{-1}) (B) and N_2O saturation level ($\%N_2O$ in %) (C) in 22 ponds in the city of Brussels during 4 seasons. Dashed lines indicate the equilibrium with atmosphere (493 ppm for pCO_2 (mean of measurements) and 100% for $\%N_2O$). Box plots show median (horizontal line), mean (cross), and 25-75% percentiles (box limits). Whiskers extend from min to max. The common letters above the box plots indicate groups that are not significantly different (Permanova). Statistical results of Permanova and Betadisper are summarized in Table S5.

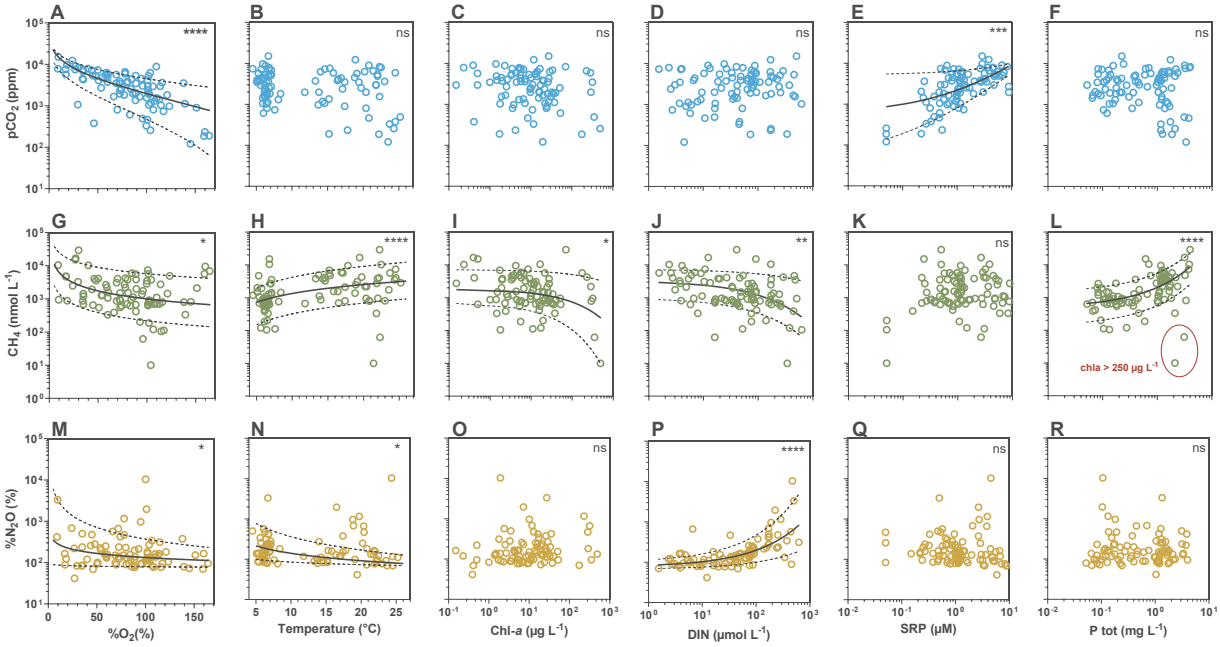

Figure 4 : Partial pressure of CO_2 (pCO_2, ppm), dissolved CH_4 concentration (CH_4, nmol L^{-1}), and N_2O saturation level ($\%N_2O$, %), versus oxygen saturation level ($\%O_2$, %), water temperature (°C), concentration of chlorophyll-*a* (Chl-*a*, in µg L^{-1}), concentration of dissolved inorganic nitrogen (DIN= NH_4^+ + NO_2^- + NO_3^- , in µmol L^{-1}), concentration of soluble reactive phosphorus (SRP, in µmol L^{-1}) and total phosphorus concentration (P tot, mg L^{-1}) in 22 ponds in the city of Brussels during 4 seasons. Median quantile regression shown as solid lines, 25th-75th quantile regression as dashed lines. Significance indicated by ns (non-significant) * ($p<0.05$), ** ($p<0.01$), ****($p<0.0001$). Statistical results of quantile regressions are summarized in Table S7.

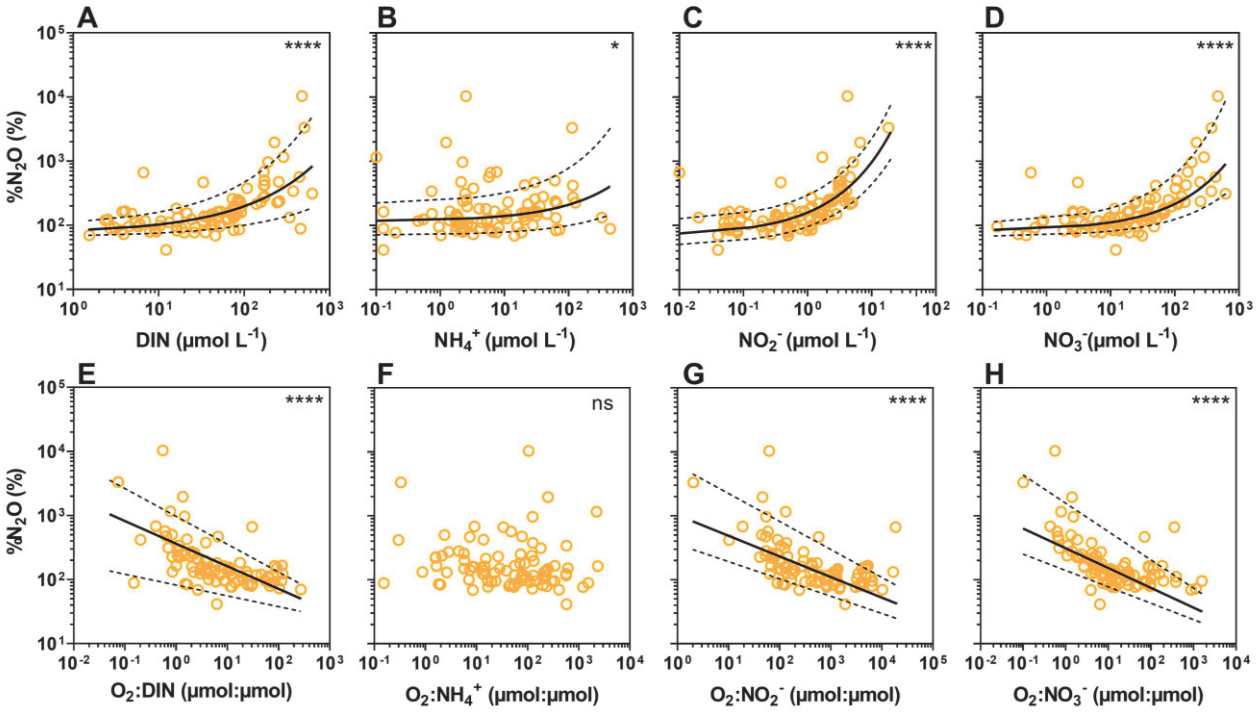

Figure 5 : N_2O saturation level (%N_2O, %) versus dissolved inorganic nitrogen (DIN= NH_4^+ + NO_2^- + NO_3^- , in µmol L^{-1}) (A), ammonium concentration (NH_4^+, µmol L^{-1}) (B), nitrite concentration (NO_2^-, µmol L^{-1}) (C), nitrate concentration (NO_3^-, µmol L^{-1}) (D), ratio of dissolved inorganic nitrogen (DIN= NH_4^+ + NO_2^- + NO_3^- , in µmol L^{-1}) to dissolved oxygen (O_2, in µmol L^{-1}) (E), ratio of NH_4^+ to O_2 (µmol:µmol) (F), ratio of NO_2^- to O_2 (µmol:µmol) (G), ratio of NO_3^- to O_2 (µmol:µmol) (H) in 22 sampled ponds in the city of Brussels during 4 seasons. Median quantile regression shown as solid lines, 25th-75th quantile regression as dashed lines. Significance indicated by * ($p<0.05$), ****($p<0.0001$). Statistical results of quantile regressions are summarized in Table S6.

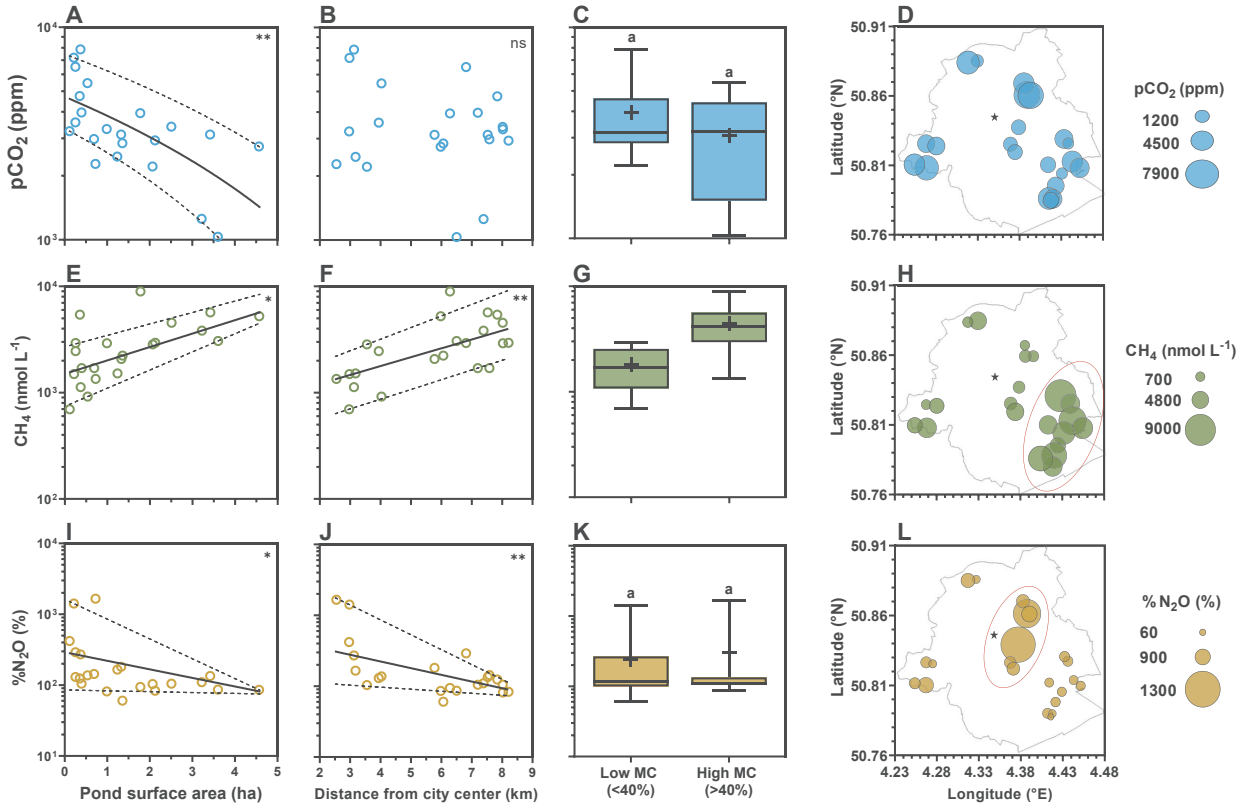

Figure 6 : Median quantile regressions of mean partial pressure of CO_2 (pCO_2, ppm), dissolved CH_4 concentration (CH_4, nmol L^{-1}), and N_2O saturation level ($\%N_2O$, %) as function of surface area (A, E, I) and distance from city center (B,F, J) and boxplots of mean GHG with low (<40%, n=14) and high (>40%, n=8) macrophyte cover (MC) (C,G, K). Median quantile regression shown as solid lines, 25th-75th quantile regression as dashed lines. Significance indicated by ns (non-significant) * ($p<0.05$), ** ($p<0.01$). Box plots show median (horizontal line), mean (cross), and 25-75% percentiles (box limits). Whiskers extend from min to max. The common letters above the box plots indicate groups that are not significantly different (Permanova). Graphs D, H, L represent respectively mean pCO_2 (ppm), CH_4, (nmol L^{-1}) and $\%N_2O$ (%) for each pond during the four spatial surveys plotted against coordinates (°E,°N). City perimeter shown in light grey, city center (50.8504°N, 4.3487°E) marked with star. Red circles evidence zones with highest values of CH_4 concentrations and $\%N_2O$. Statistical results of Permanova and Betadisper are summarized in Table S6. Statistical results of quantile regressions are summarized in Table S7.

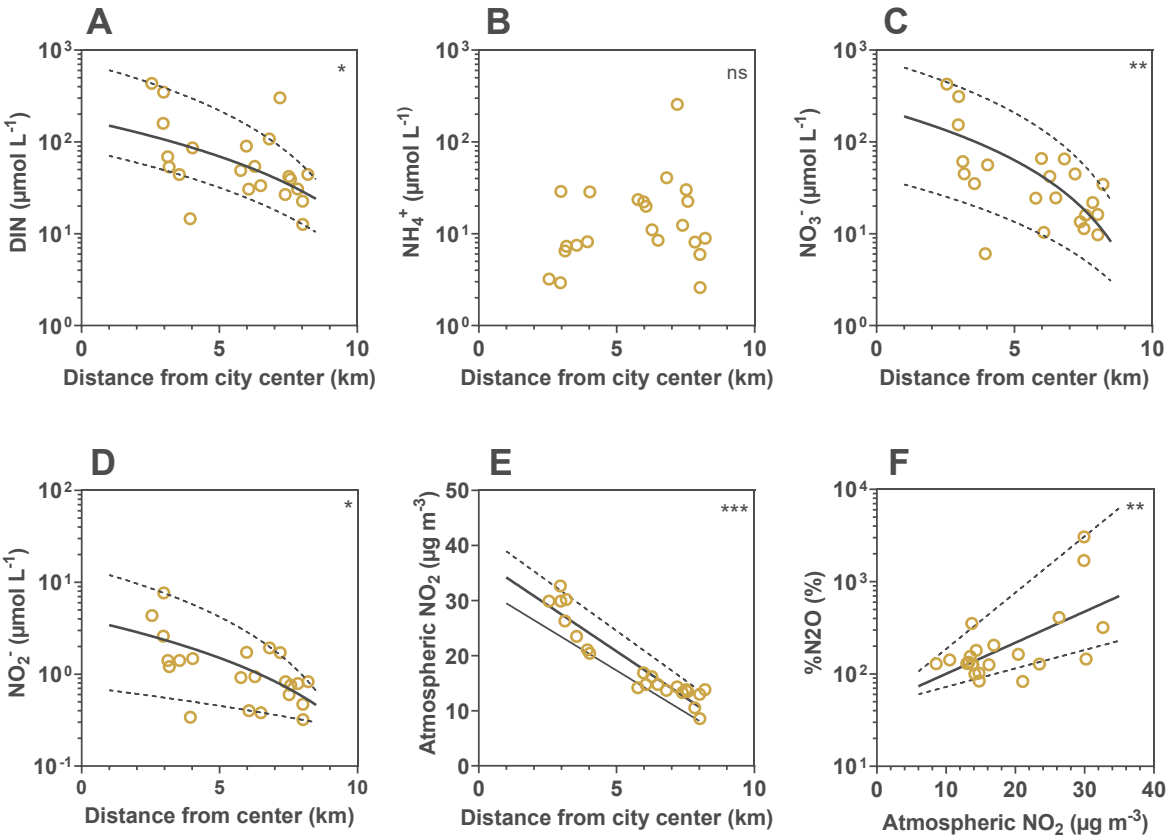

Figure 7 : Mean dissolved inorganic nitrogen (DIN= NH_4^+ + NO_2^- + NO_3^- , in µmol L^{-1}) (A), ammonium (NH_4^+, in µmol L^{-1}) (B), nitrite (NO_2^-, in µmol L^{-1}) (C), nitrate (NO_3^-, in µmol L^{-1}) (D), and atmospheric NO_2 (µg m^{-3}) (E) concentrations as function of the distance from city center (50.8504°N, 4.3487°E) in 22 ponds in the city of Brussels during 4 seasons. N_2O saturation level (%N_2O, %) as function of atmospheric NO_2 concentration (µg m^{-3}) (F). Median quantile regression shown as solid lines, 25th-75th quantile regression as dashed lines. Significance (ns non-significant, * $p<0.05$, ** $p<0.01$) indicated top right. Statistical results of quantile regressions are summarized in Table S6. The atmospheric nitrogen dioxide (NO_2) concentration (µg m^{-3}) was extracted from the Curieuzenair initiative, which analyzed 2483 air samples in September 2021 covering the whole of the city of Brussels with a homogeneous distribution (https://curieuzenair.brussels/en/the-results/). Each data point corresponds to the average value of the six atmospheric NO_2 stations closest to each sampled pond, a distance between 50 and 450m.

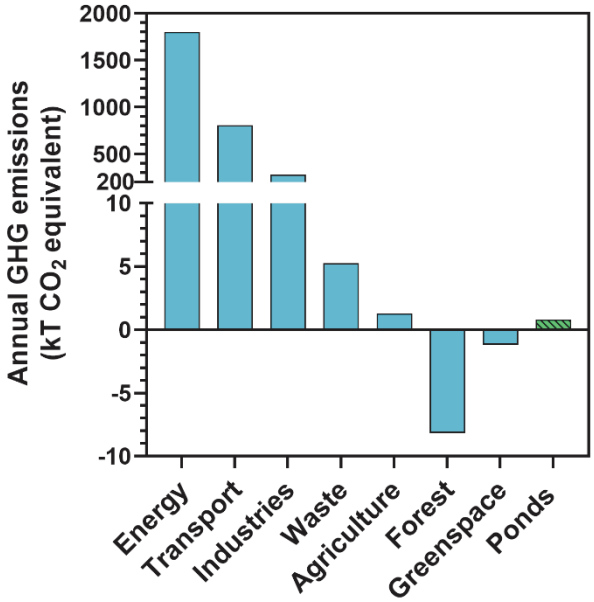

Figure 8 : Official inventory of annual emissions of greenhouse gases (kT CO_2 equivalents per year) for the city of Brussels in 2020 (https://environnement.brussels) Energy (residential/tertiary buildings), Transport (road), Industry (industrial processes and product use), Waste (mainly wastewater treatment), Agriculture (few soils), Forest (mainly Sonian forest), greenspace (private and public gardens, grassland) and diffusive emissions estimated from Brussels ponds (Ponds) in this study (2021-2022). The specific budget for each GHG is given in Table S4.

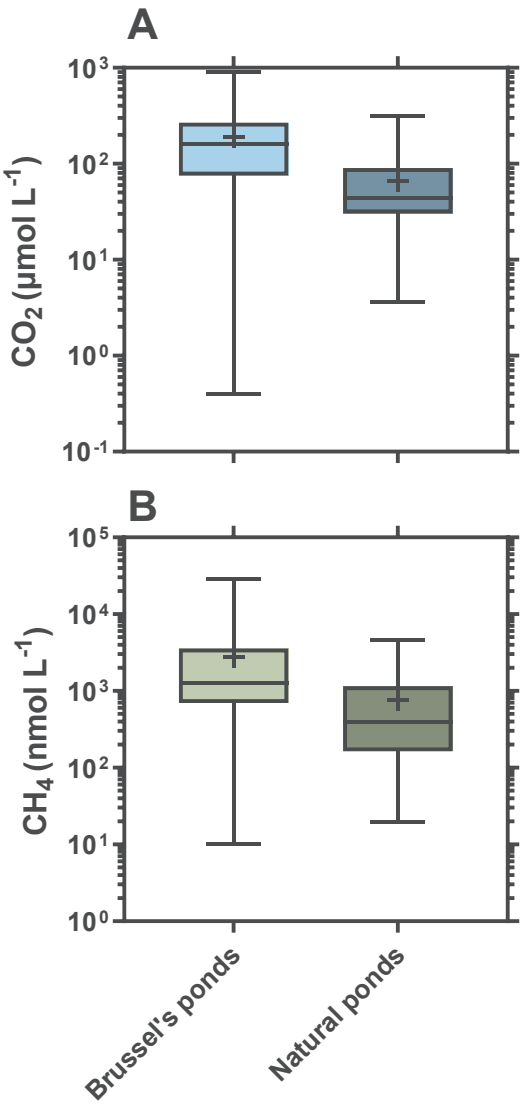

Figure 9: dissolved CO_2 concentration (CO_2, µmol L^{-1}) (A) and dissolved CH_4 concentration (CH_4, nmol L^{-1}) (B) in 22 sampled ponds in Brussels during 4 seasons (n=88) and natural ponds of similar size reported by Holgerson and Raymond (2016) (n=81 for CO_2, n=53 for CH_4). Box plots show median (horizontal line), mean (cross), and 25-75% percentiles (box limits). Whiskers extend from min to max. Both comparisons are significant based on Permanova test. Statistical results of Permanova and Betadisper are summarized in Table S5.

Seasonal and spatial variations of greenhouse gas (CO_2, CH_4 and N_2O) emissions from urban ponds in Brussels

(Supplementary Tables and figures)

Bauduin T.[1,2,*], Gypens N.[1], Borges A.V.[2]

[1] Ecology of Aquatic Systems, Free University of Brussels, Belgium

[2] Chemical Oceanography Unit, University of Liège, Belgium

thomas.bauduin@ulb.be

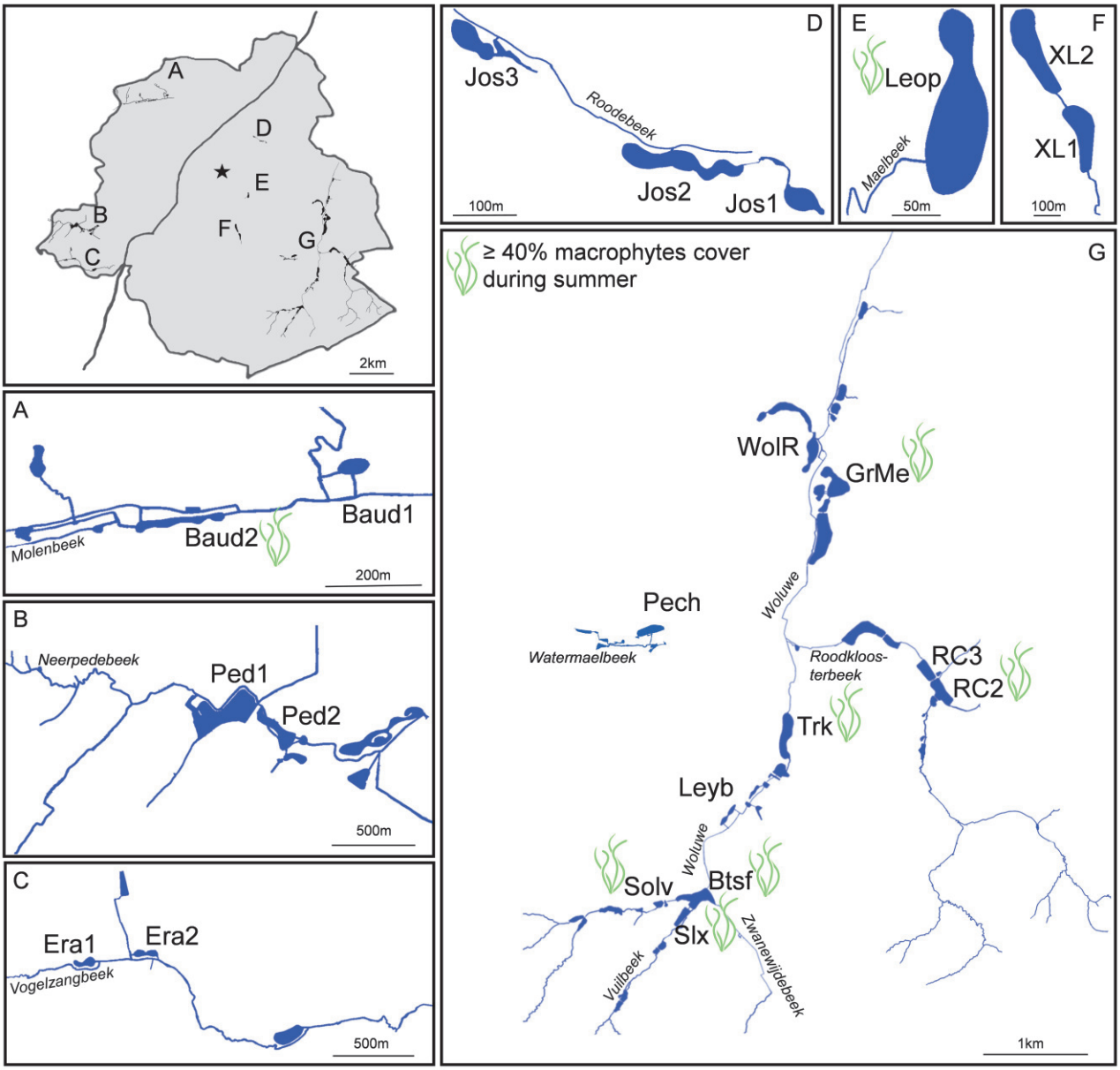

Figure S1 : Map of the city of Brussels and the sampled ponds. The acronyms correspond to the official names of the ponds of Bruxelles Environnement, the regional water management agency (Baud 1 : Etang Parc Roi Baudouin Phase I ; Baud2 : Etang Parc Roi Baudouin Phase II ; Btsf : Etang de Boitsfort ; Era 1 : Etang Erasme amont ; Era 2 : Etang Erasme aval ; GrMe : Grand étang Mellaerts ; Jos1 : Parc Josaphat - Etang aux canards ; Jos2 : Parc Josaphat – Etang aux pigeons ; Jos3 : Parc Josaphat – Etang de la laiterie ; Leop : Etang parc Leopold ; Leyb : Etang du Leybeek ; Pech : Etang Pêcheries Royales ; Ped1 : Etang de la Pède Grand Etang ; Ped2 : Etang de la Pède ; RC2 : Grand étang des Clabots (Etang 2) ; RC3 : Etang du moulin (Etang 3) ; Slx : Etang du Silex ; Solv : Grand étang – Parc Tournay Solvay ; Trk : Etang Parc Ten Reuken ; WolR : Etang rond – Parc de Woluwe ; XL1 : Etang d'Ixelles Nord ; XL2 : Etang d'Ixelles Sud). The stream names are italicized. The city center (50.8504°N, 4.3487°E) is marked with star.

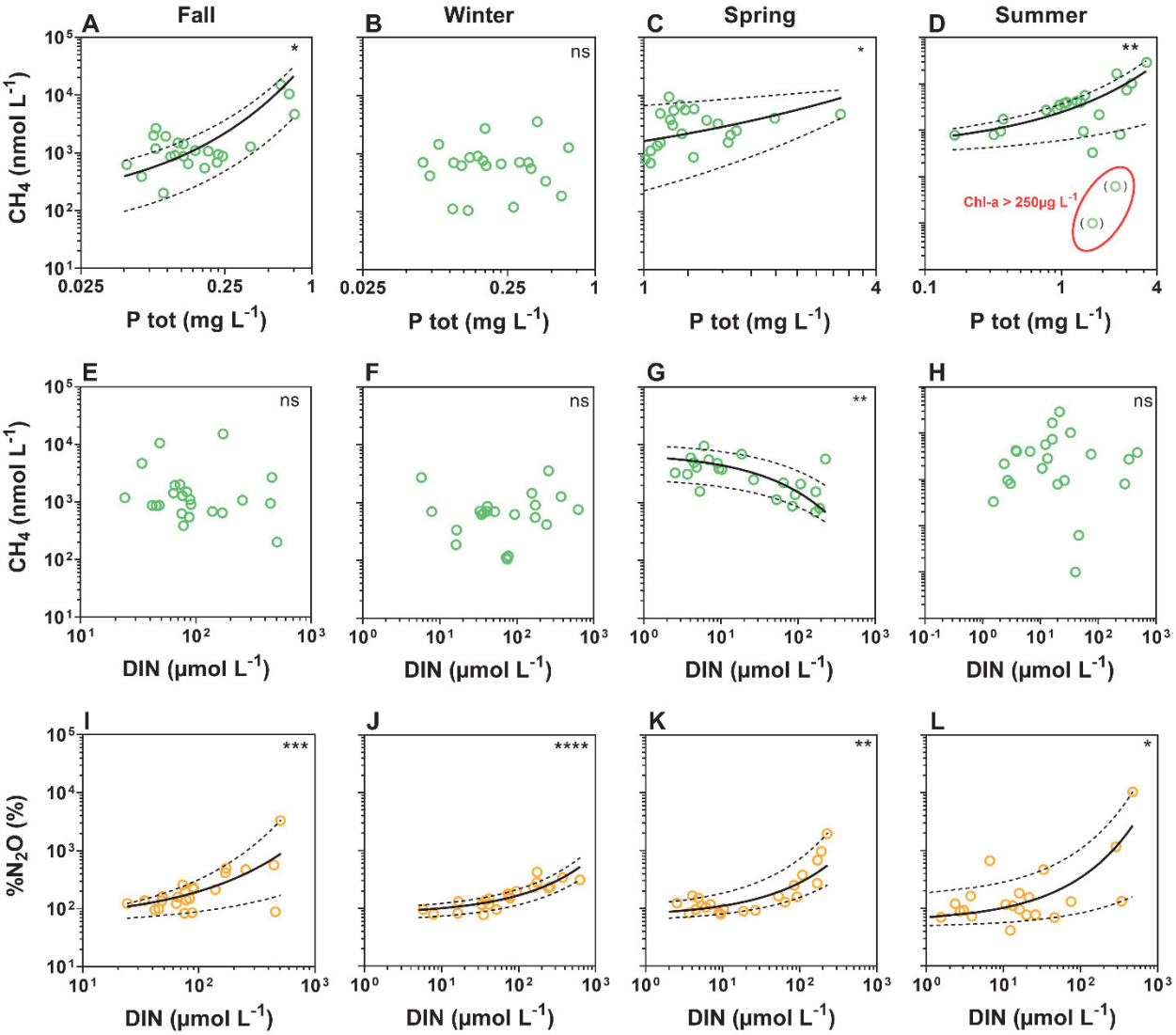

Figure S2: Dissolved CH4 concentration (CH_4, nmol L^{-1}) versus the total phosphorus concentration (P tot, mg L^{-1}) (A,B,C,D) and versus dissolved inorganic nitrogen (DIN= NH_4^+ + NO_2^- + NO_3^- , in µmol L^{-1}) (E,F,G,H), N_2O saturation level (%N_2O, %) versus dissolved inorganic nitrogen (DIN= NH_4^+ + NO_2^- + NO_3^- , in µmol L^{-1}) (I,J,K,L) in 22 sampled ponds in the city of Brussels during 4 seasons. Median quantile regression shown as solid lines, 25th-75th quantile regression as dashed lines. Significance indicated by ns (non-significant) * ($p<0.05$), ** ($p<0.01$), ***($p<0.001$), ****($p<0.0001$). Statistical results of quantile regressions are summarized in Table S6.

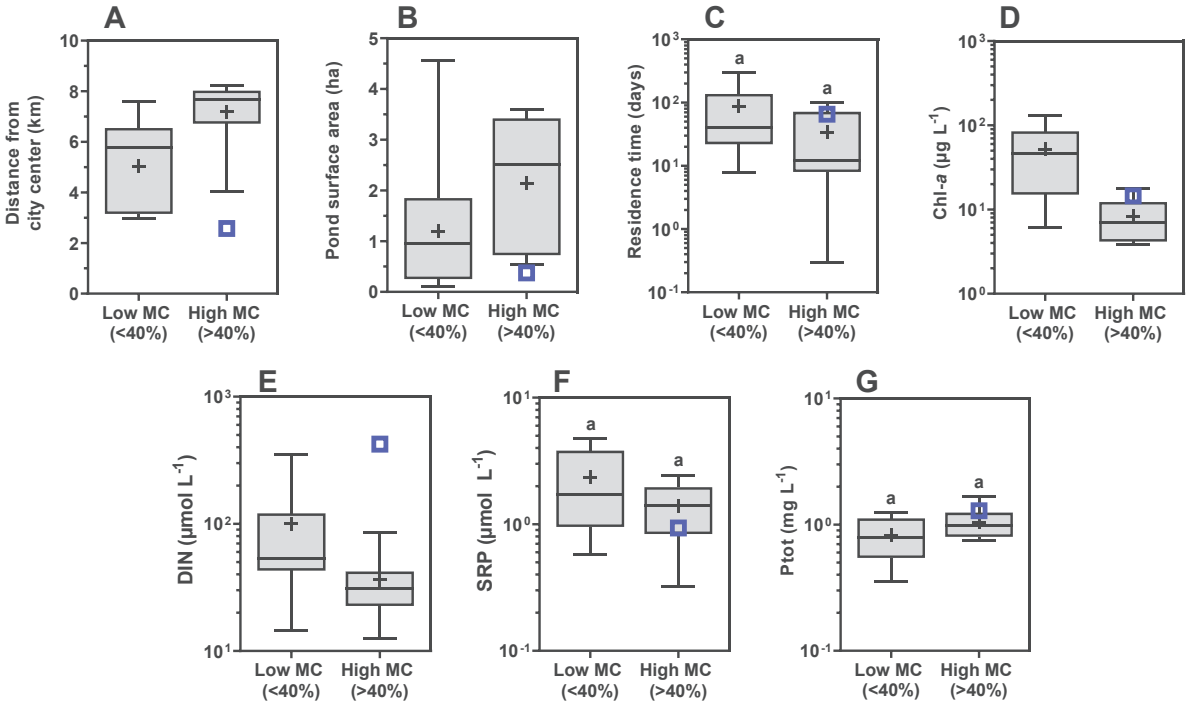

Figure S3: Distance from city center (km) (A), pond surface (ha) (B), pond water residence time (days) (C), mean chlorophyll-a (µg L^{-1}) (D), dissolved inorganic nitrogen (DIN= NH_4^+ + NO_2^- + NO_3^- , in µmol L^{-1}) (E), soluble reactive phosphorus (SRP, in µmol L^{-1}) (F), total phosphorus (Ptot, in mg L^{-1}) (G), in 22 ponds with macrophyte cover below and above 40% during four seasons in the city of Brussels. Leopold Pond is indicated by an empty blue square and was excluded from the analysis due to extreme values for some variables. Box plots show median (horizontal line), mean (cross), and 25-75% percentiles (box limits). Whiskers extend from min to max. The common letters above the box plots indicate groups that are not significantly different (Permanova). Statistical results of Permanova and Betadisper are summarized in Table S6.

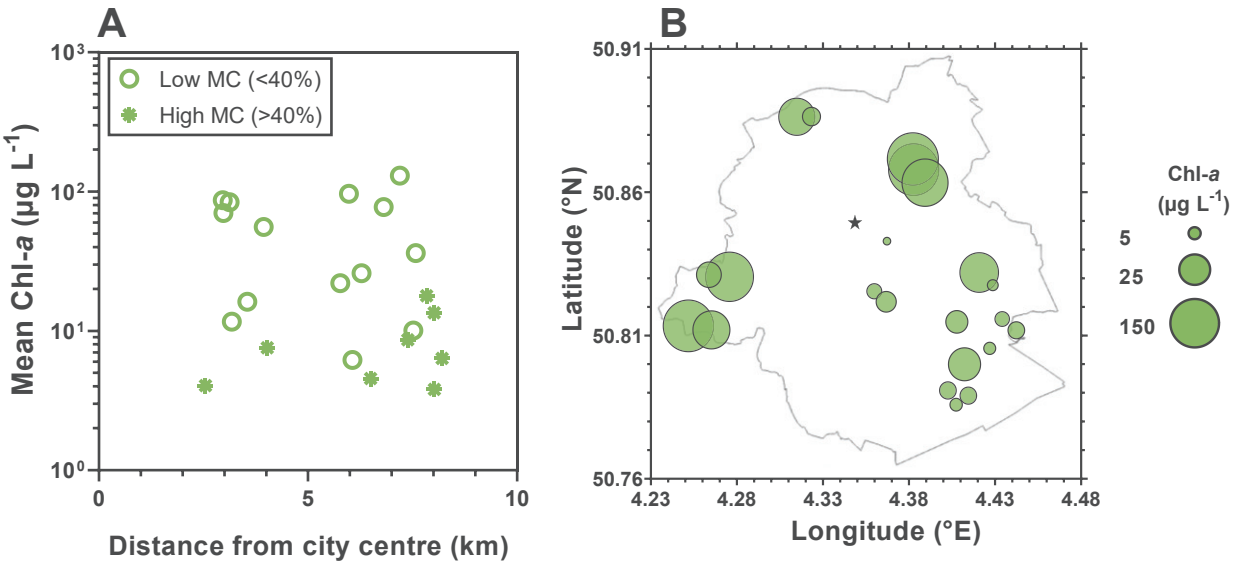

Figure S4: Mean chlorophyll-*a* concentration (Mean Chl-*a*, in µg L^{-1}) in 22 sampled ponds during the four seasons in the city of Brussels as a function of the distance from city center (50.8504°N, 4.3487°E) (A) and on a map showing the city perimeter (line) and center (star, 50.8504°N, 4.3487°E) (B).

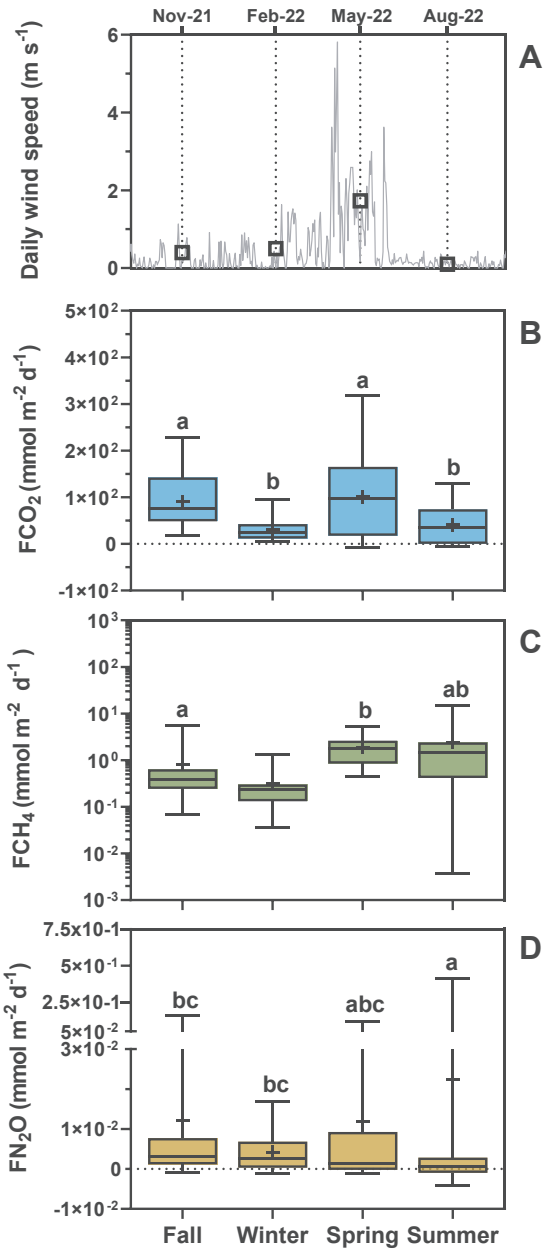

Figure S5 : Daily wind speed (dark grey, m s^{-1}) obtained from crowdsourcing platform of the Royal Belgian Meteorological Institute (wow.meteo.be) at the Brussels – Woluwe Saint Lambert station (50.8408 °N, 4.4234 °E) (A). squares indicate the mean wind for all samplings during a campaign. Seasonal comparisons of diffusive fluxes of CO_2 (B), CH_4 (C) and N_2O (D) (mmol m^{-2} d^{-1}) in 22 ponds in the city of Brussels during 4 seasons. Box plots show median (horizontal line), mean (cross), and 25-75% percentiles (box limits). Whiskers extend from min to max. The common letters above the box plots indicate groups that are not significantly different (Permanova). Statistical results of Permanova and Betadisper are summarized in Table S4.

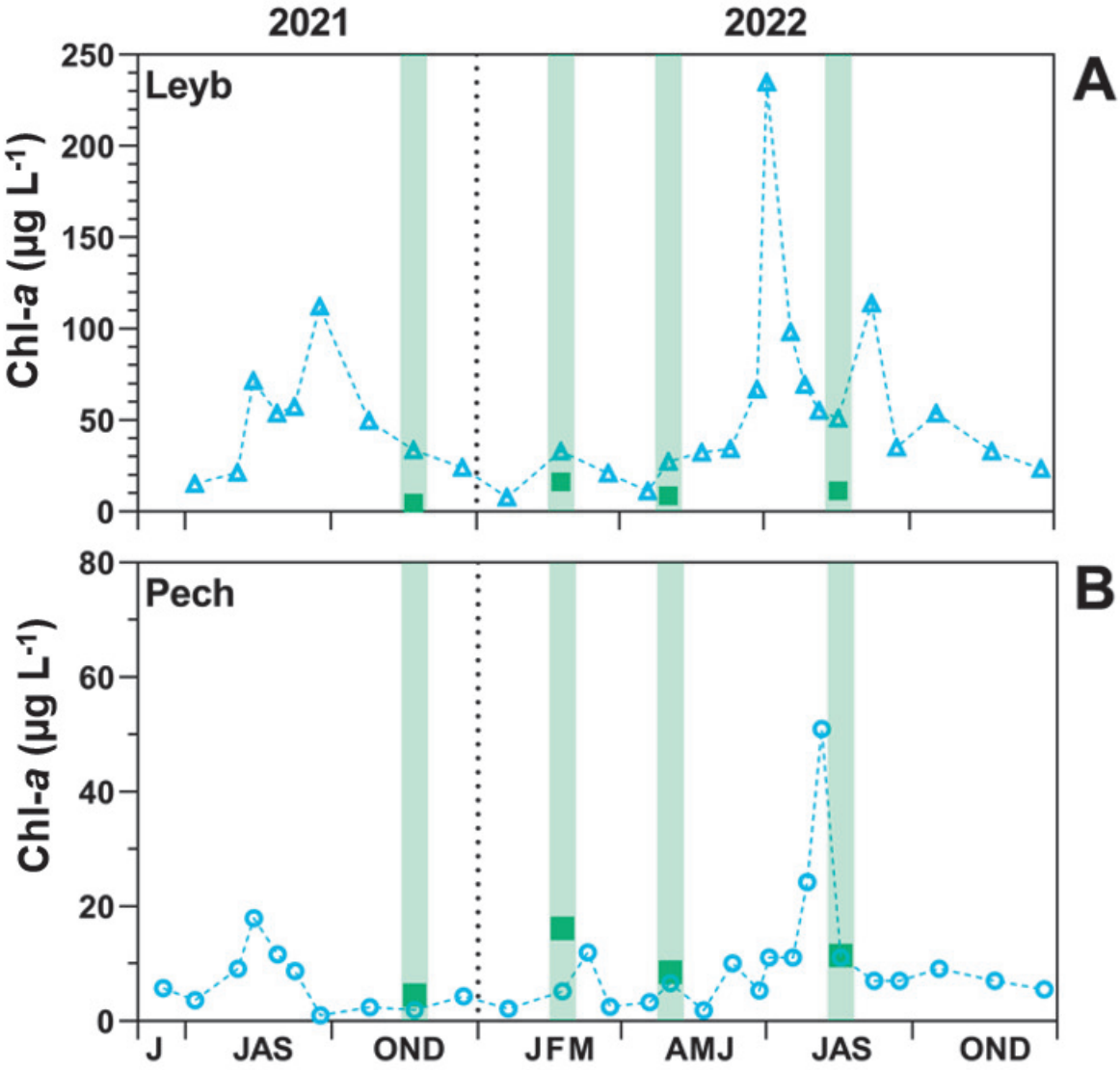

Figure S6: Chlorophyll-a concentration in (Chl-*a*, in µg L^{-1}) in the Leybeek (Leyb) (A) and Pêcheries (Pech) (B) ponds from June 2021 to December 2022. The solid squares indicate the median values of the 22 ponds sampled at four different seasons.

Table S1: Name, acronym, catchment, geographical coordinates, surface area, depth, perimeter, residence time, distance from the city center (50.8504°N, 4.3487°E), summer macrophyte cover, over-flow or flow-through regime, fishing activity, and storm-water regulation in 22 ponds in the city of Brussels. Surface area and perimeter data were calculated from satellite images in Google Earth and the other data were obtained from data resources from Brussels Environment, the regional water management agency.

Pond name (in French, according to Bruxelles Environnement)	Abbreviation	Catchment	Latitude (°N)	Longitude (°E)	Average depth (m)	Surface (ha)	Perimeter (m)	Residence time (days)	Distance from city center (km)	Summer macrophyte cover (%)	Regime	Fishing pond	Build as Stormwater Pond
Etang Parc Roi Baudouin Phase I (Sacré Cœur)	Baud1	Molenbeek	50.8833	4.3276	0.8	0.3	211	30.0	3.9	25	Overflow	No	No
Etang Parc Roi Baudouin Phase II - Sud	Baud2	Molenbeek	50.8813	4.3185	0.8	0.5	671	100.0	4.0	60	Overflow	No	No
Etang de Boitsfort ou du Moulin	Btsf	Woluwe	50.7930	4.4171	0.3	2.5	904	7.0	8.0	60	Flow-through	No	No
Etang Erasme Amont	Era1	Neerpedebeek	50.8118	4.2666	0.7	0.4	316	45.0	7.2	25	Overflow	No	Yes
Etang Erasme Aval	Era2	Neerpedebeek	50.8123	4.2722	0.7	0.3	283	30.0	6.8	5	Overflow	No	Yes
Grand étang Mellaerts	GrMe	Woluwe	50.8274	4.4347	1.2	3.6	939	78.0	6.5	50	Overflow	No	No
Parc Josaphat - Etang aux canards	Jos1	Maelbeek	50.8606	4.3903	0.5	0.4	438	115.0	3.1	0	Overflow	No	No
Parc Josaphat - Etang aux pigeons	Jos2	Maelbeek	50.8611	4.3878	0.6	0.2	206	66.4	3.0	15	Overflow	No	No
Parc Josaphat - Etang de la laiterie	Jos3	Maelbeek	50.8629	4.3830	0.7	0.1	481	35.9	3.0	15	Overflow	No	No
Etang Parc Leopold	Leop	Maelbeek	50.8390	4.3802	1.0	0.7	515	150.0	2.5	50	Overflow	No	No
Etang Parc du Leybeek	Leyb	Woluwe	50.8000	4.4210	0.6	0.7	511	300.0	7.6	0	Overflow	No	No
Etang Pêcheries Royales - Parc de la Héronnière	Pech	Woluwe	50.8127	4.4119	1.3	1.4	558	7.8	6.1	15	Flow-through	Yes	No
Etang de la Pède - Grand Etang	Ped1	Neerpedebeek	50.8262	4.2726	1.3	4.6	1084	25.0	6.0	30	Overflow	No	Yes
Etang de la Pede	Ped2	Neerpedebeek	50.8254	4.2766	0.7	1.3	713	100.0	5.8	20	Overflow	No	Yes
Grand étang des Clabots (Etang 2) - Rouge-Cloître	RC2	Woluwe	50.8105	4.4477	2.0	2.1	664	13.0	8.2	25	Flow-through	No	No
Etang du Moulin (Etang 3) - Rouge-Cloître	RC3	Woluwe	50.8118	4.4463	1.1	3.4	989	11.0	7.5	40	Flow-through	Yes	No
Etang du Silex	Slx	Woluwe	50.7917	4.4151	1.1	1.0	464	0.3	8.0	90	Flow-through	No	No
Grand étang - Parc Tournay-Solvay	Solv	Woluwe	50.7925	4.4123	1.4	0.4	331	12.0	7.8	80	Flow-through	No	No
Etang Parc Ten Reuken	Trk	Woluwe	50.8066	4.4278	1.4	3.2	1148	12.0	7.4	80	Flow-through	No	No
Etang rond - Parc de Woluwe	WolR	Woluwe	50.8300	4.4317	1.4	1.8	600	10.7	6.3	15	Overflow	No	No
Etang d'Ixelles Nord	XL1	Maelbeek	50.8229	4.3743	1.8	2.1	774	200.0	3.5	20	Flow-through	Yes	No
Etang d'Ixelles Sud	XL2	Maelbeek	50.8257	4.3716	1.2	1.2	589	250.0	3.2	15	Flow-through	Yes	No

Table S2: Mean, standard deviation (SD), minimal value (min), maximal value (max), median and interquartile range (IQR) and number of samples (n) of Water temperature (in °C), pH, conductivity (in µS cm^{-1}), Oxygen saturation (in %), Ammonium, Nitrite, Nitrate, Soluble reactive phosphorus (SRP) concentrations (in µmol L^{-1}), total phosphorus concentration (in mg L^{-1}), Chlorophyll-a concentration (in µg L^{-1}), total suspended matter concentration (in mg L^{-1}), partial pressure of CO_2 (pCO_2 in ppm); dissolved CH_4 concentration (CH_4 in nmol L^{-1}) and N_2O saturation level (in %) measured at 22 ponds in the city of Brussels during 4 seasons. Statistical results of Permanova and Betadisper for comparisons between seasons are summarized in Table S4.

November 2021					
Parameter	**Units**	**mean ± SD**	**(min;max)**	**median (IQR)**	**n**
Water temperature	°C	6.1 ± 0.7	(4.5 ; 7.1)	6.2 (5.5 ; 6.6)	22
pH		7.51 ± 0.42	(7.12 ; 8.23)	7.39 (7.19 ; 7.74)	22
Conductivity	µS cm^{-1}	858 ± 256	(599 ; 1507)	795 (675 ; 918)	22
Oxygen saturation	%	52 ± 29	(9 ; 110)	51 (34.6 ; 70.9)	22
Ammonium	µmol L^{-1}	57.7 ± 90.4	(2.1 ; 447.0)	29.8 (20.4 ; 62.6)	22
Nitrite	µmol L^{-1}	2.7 ± 3.6	(0.6 ; 18.3)	1.7 (1.2 ; 2.9)	22
Nitrate	µmol L^{-1}	77.2 ± 115.4	(9.3 ; 432.8)	34.6 (21.1 ; 47.4)	22
SRP	µmol L^{-1}	1.8 ± 1.2	(0.5 ; 4.8)	1.2 (1.0 ; 2.8)	22
Total phosphorus	mg L^{-1}	0.1 ± 0.2	(0.1 ; 0.8)	0.1 (0.1 ; 0.3)	22
Chlorophyll-a	µg L^{-1}	9.5 ± 10.0	(0.5 ; 33.6)	4.5 (2.1 ; 15.2)	22
Total suspended matter	mg L^{-1}	8.3 ± 14.2	(1.2 ; 72.4)	4.6 (3.9 ; 7.6)	22
pCO_2	ppm	5453 ± 3058	(1655 ; 15029)	4650 (3568 ; 7094)	22
CH_4	nmol L^{-1}	2260 ± 3523	(201 ; 15132)	1073 (773 ; 1714)	22
N_2O saturation	%	360 ± 677	(84 ; 3324)	161 (123 ; 247)	22
February 2022					
Water temperature	°C	6.9 ± 1.3	(5.6 ; 11.8)	6.5 (6.2 ; 7.1)	21
pH		8.11 ± 0.47	(7.05 ; 8.75)	8.13 (7.93 ; 8.49)	21
Conductivity	µS cm^{-1}	796 ± 265	(520 ; 1364)	685 (585 ; 942)	21
Oxygen saturation	%	96 ± 23	(48 ; 139)	102 (80 ; 111)	21
Ammonium	µmol L^{-1}	12.3 ± 27.9	(0.7 ; 127.6)	2.6 (1.9 ; 7.5)	21
Nitrite	µmol L^{-1}	1.6 ± 1.5	(0.1 ; 5.0)	1.1 (0.5 ; 3.1)	21
Nitrate	µmol L^{-1}	110.3 ± 146.6	(4.6 ; 619.3)	65.2 (30.8 ; 129.5)	21
SRP	µmol L^{-1}	2.2 ± 2.9	(0.2 ; 8.9)	0.6 (0.4 ; 2.0)	21
Total phosphorus	mg L^{-1}	0.3 ± 0.2	(0.1 ; 0.7)	0.2 (0.2 ; 0.4)	21
Chlorophyll-a	µg L^{-1}	19.7 ± 14.3	(1.8 ; 52.8)	16.2 (7.2 ; 30.7)	21
Total suspended matter	mg L^{-1}	9.5 ± 4.5	(3.7 ; 20.3)	9.2 (5.7 ; 11.1)	21
pCO_2	ppm	2064 ± 1295	(610 ; 5283)	1822 (1121 ; 2524)	21
CH_4	nmol L^{-1}	860 ± 841	(105 ; 3552)	697 (416 ; 861)	21
N_2O saturation	%	182 ± 95	(77 ; 425)	150 (117 ; 231)	20
May 2022					
Water temperature	°C	16.2 ± 2.0	(13.3 ; 20.2)	16.1 (14.6 ; 17.4)	22
pH		8.06 ± 0.50	(7.37 ; 9.12)	7.91 (7.72 ; 8.44)	22
Conductivity	µS cm^{-1}	776 ± 272	(402 ; 1424)	709 (604 ; 835)	22
Oxygen saturation	%	90 ± 41	(17 ; 164)	87 (61 ; 104)	22
Ammonium	µmol L^{-1}	10.9 ± 25.0	(0.5 ; 117.6)	2.9 (1.8 ; 7.5)	22
Nitrite	µmol L^{-1}	1.3 ± 1.8	(0.1 ; 6.6)	0.4 (0.1 ; 1.8)	22
Nitrate	µmol L^{-1}	45.5 ± 64.9	(0.9 ; 218.0)	10.7 (2.9 ; 69.5)	22
SRP	µmol L^{-1}	1.6 ± 1.5	(0.2 ; 5.6)	1.0 (0.8 ; 1.2)	22
Total phosphorus	mg L^{-1}	1.4 ± 0.5	(1.0 ; 3.3)	1.3 (1.1 ; 1.6)	22
Chlorophyll-a	µg L^{-1}	11.9 ± 8.8	(1.7 ; 29.0)	8.5 (5.2 ; 19.2)	22
Total suspended matter	mg L^{-1}	10.7 ± 7.4	(3.2 ; 38.5)	8.3 (7.3 ; 12.1)	22
pCO_2	ppm	3892 ± 2993	(190 ; 12329)	3787 (1218 ; 5805)	22
CH_4	nmol L^{-1}	3456 ± 2301	(688 ; 9507)	3180 (1546 ; 4790)	22
N_2O saturation	%	289 ± 432	(79 ; 1963)	125 (96 ; 250)	22
August 2022					
Water temperature	°C	22.2 ± 1.6	(19.4 ; 25.2)	22.1 (20.8 ; 23.3)	22
pH		7.99 ± 0.56	(7.08 ; 9.10)	7.90 (7.65 ; 8.25)	22
Conductivity	µS cm^{-1}	667 ± 270	(435 ; 1557)	537 (499 ; 792)	22
Oxygen saturation	%	87 ± 33	(27 ; 159)	93 (71 ; 101)	22
Ammonium	µmol L^{-1}	23.7 ± 70.1	(0.1 ; 330.6)	3.0 (0.7 ; 15.0)	22
Nitrite	µmol L^{-1}	0.4 ± 0.9	(0.0 ; 4.2)	0.1 (0.0 ; 0.4)	22
Nitrate	µmol L^{-1}	42.1 ± 112.4	(0.2 ; 467.7)	7.8 (1.7 ; 11.8)	22
SRP	µmol L^{-1}	2.6 ± 2.6	(0.1 ; 8.4)	1.4 (0.4 ; 4.2)	22
Total phosphorus	mg L^{-1}	2.0 ± 1.4	(0.2 ;5.3)	1.8 (1.2 ; 2.8)	22
Chlorophyll-a	µg L^{-1}	105.9 ± 149.9	(0.1 ; 488.4)	11.4 (2.8 ; 201.9)	22
Total suspended matter	mg L^{-1}	33.2 ± 37.4	(3.2 ; 110.2)	12.1 (6.1 ; 59.3)	22
pCO_2	ppm	3185 ± 2902	(121 ; 8970)	2737 (469 ; 5218)	22
CH_4	nmol L^{-1}	4691 ± 6713	(10 ; 29190)	2790 (883 ; 4956)	22
N_2O saturation	%	656 ± 2182	(0 ; 10354)	113 (77; 159)	22
All seasons					
Water temperature	°C	12.8 ± 6.9	(4.5 ; 25.2)	12.6 (6.4 ; 19.5)	87
pH		7.91 ± 0.53	(7.05 ; 9.12)	7.87 (7.55 ; 8.20)	87
Conductivity	µS cm^{-1}	775 ± 271	(402 ; 1557)	699 (580 ; 903)	87
Oxygen saturation	%	81 ± 36	(9 ; 164)	83 (54 ; 103)	87
Ammonium	µmol L^{-1}	26.7 ± 62.9	(0.1 ; 447.0)	5.6 (2.1 ; 24.0)	87
Nitrite	µmol L^{-1}	1.5 ± 2.3	(0.0 ; 18.3)	0.8 (0.2 ; 2.1)	87
Nitrate	µmol L^{-1}	68.4 ± 114.6	(0.2 ; 619.3)	24.8 (7.0 ; 66.7)	87
SRP	µmol L^{-1}	2.0 ± 2.2	(0.1 ; 8.9)	1.1 (0.6 ; 2.9)	87
Total phosphorus	mg L^{-1}	1.0 ± 1.1	(0.1 ; 5.3)	0.6 (0.15 ; 1.4)	87
Chlorophyll-a	µg L^{-1}	36.6 ± 84.6	(0.1 ; 488.4)	10.0 (3.6 ; 24.9)	87
Total suspended matter	mg L^{-1}	15.5 ± 22.8	(1.2 ; 110.2)	8.0 (5.2 ; 11.8)	87
pCO_2	ppm	3667 ± 2904	(121 ; 15029)	3016 (1394 ; 5343)	87
CH_4	nmol L^{-1}	2833 ± 4178	(10 ; 29190)	1276 (705 ; 3604)	87
N_2O saturation	%	273 ± 662	(0 ; 10354)	138 (96 ; 232)	86

Table S3: Dissolved concentrations of CO_2, CH_4 and N_2O in urban ponds reported in literature and the present study in 22 urban ponds in the city of Brussels during 4 seasons.

Region	n	Coverage	CO_2	CH_4	N_2O	Reference
			(µmol L^{-1})	(nmol L^{-1})	(nmol L^{-1})	
Brussel (Belgium)	22	4 seasons	189 ± 155	2,745 ± 4,120	39 ± 95	This study
Brussel (Belgium)	22	Summer	123 ± 112	4,691 ± 6,713	8 ± 158	This study
Linkoping (Sweden)	1	4 seasons	-	1,733	-	Natchimuthu et al. (2014)
Minnesota (United Sates)	7	Summer	6 ± 180	2,530 ± 32,360		Ray et al. (2023)
Minnesota (United States)	18	Summer	170 ± 180	15,794 ± 23,107	18 ± 12	Rabaey and Cotner (2022)
Salaspils (Lativa)	1	Summer	133 ± 17	4,914 ± 3,779		Ray et al. (2023)
Silkeborg (Denmark)	37	4 seasons	162 ± 184	3,667 ± 16,500	28 ± 64	Audet et al. (2020)
Silkeborg (Denmark)	37	Summer	202 ± 302	6,000 ± 32,200	-	Audet et al. (2020)
Uppsala (Sweden)	40	Summer	157 ± 153	4,528 ± 5,712	-	Peacock et al. (2019)
Uppsala (Sweden)	2	Summer	66 ± 74	804 ± 2,378		Ray et al. (2023)

Table S4 : Reported annual emissions of CO_2, CH_4, and N_2O in CO_2 equivalents from the Brussels region for the year 2020 (https://environnement.brussels) and the CO_2, CH_4 and N_2O emissions from the urban ponds (n=158, total area = 101ha), and their relative contribution. The CH_4 emissions have a diffusive component (Diff.) computed from the diffusive flux estimates in the 22 ponds during the 4 seasons, and an ebullitive component (Ebull.) computed from water temperature in the 22 ponds during the 4 seasons based on a relation between CH_4 ebullition and water temperature collected in 4 ponds (Leybeek, Pêcheries, Silex and Ten Reuken) from 2021-2023 (unpublished data).

		CO_2	CH_4	N_2O
		kT CO_2 eq y^{-1}		
Officially reported	Energy	1796.18	6.15	1.63
	Transport	799.01	0.73	6.87
	Industries	275.45	0.04	2.23
	Waste	0.00	0.29	4.98
	Agriculture	0.04	0.53	0.71
	Forest	-8.68	0.00	0.50
	Greenspace	-1.19	0.00	0.00
This study	Ponds	0.74	0.09 (Diff.) 0.21 (Ebull.)	0.01
			Relative contribution (%)	
Ponds (expressed as fraction of the total)		0.03	1.12 (Diff.) 2.61 (Ebull.)	0.05

Table S5: Outcomes of the Betadisper and Permanova statistical tests for pairs of seasons on the medians of Water temperature (Temperature, in °C), Oxygen saturation ($\%O_2$, in %), Soluble reactive phosphorus (SRP, in µmol L^{-1}), total phosphorus concentration (Ptot, in mg L^{-1}), ammonium concentration (NH_4^+, in µmol L^{-1}) ; nitrite concentration (NO_2^-, in µmol L^{-1}), nitrate concentration (NO_3^-, in µmol L^{-1}), dissolved inorganic nitrogen (DIN= $NH_4^+ + NO_2^- + NO_3^-$, in µmol L^{-1}), Chlorophyll-a concentration (Chl-a, in µg L^{-1}), total suspended matter concentration (TSM, in mg L^{-1}), dissolved CH_4 concentration (CH_4, in nmol L^{-1}), partial pressure of CO_2 (pCO_2, in ppm); N_2O saturation level ($\%N_2O$, in %), diffusive fluxes of CO_2 (FCO_2), CH_4 (FCH_4) and N_2O (FN_2O) (mmol m^{-2} d^{-1}). Transformations have been applied to the data to ensure a normal distribution, and are indicated in the Transformation column.

Figure or table	Variable	Transformation	p-values of the Permanova test					
			Fall vs Winter	Fall vs Spring	Fall vs Summer	Winter vs Spring	Winter vs Summer	Spring vs Summer
Tab. S2	Temperature (°C)	logarithmic	**0.005** **	**0.001** ***	**0.001** ***	**0.001** ***	**0.001** ***	**0.001** ***
	$\%O_2$ (%)	logarithmic	**0.001** ***	**0.004** **	**0.003** **	0.241	0.170	0.925
	SRP (µmol L^{-1})	square root	0.847	0.486	0.610	0.771	0.615	0.342
	P_{tot} (mg L^{-1})	square root	0.452	**0.001** ***	**0.001** ***	**0.001** ***	**0.001** ***	0.172
	NH_4^+ (µmol L^{-1})	square root	**0.002** **	**0.001** ***	**0.004** **	0.804	0.729	0.582
	NO_2^- (µmol L^{-1})	square root	**0.041** *	**0.006** **	**0.001** ***	0.218	**0.001** ***	**0.04** *
	NO_3^- (µmol L^{-1})	square root	0.354	0.119	**0.022** *	**0.015** *	**0.004** **	0.419
	DIN (µmol L^{-1})	square root	0.532	**0.003** **	**0.008** **	**0.037** *	**0.038** *	0.864
	Chl-a (µg L^{-1})	square root	**0.007** **	0.076	0.088	0.100	0.928	0.413
	TSM (mg L^{-1})	square root	**0.039***	**0.044***	**0.003** **	0.333	0.106	0.237
Fig. 3	CH_4 (nmol L^{-1})	logarithmic	**0.008** **	**0.007** **	0.092	**0.001** ***	**0.014** *	0.368
	$\%N_2O$ (%)	logarithmic	0.262	0.477	**0.024***	0.764	**0.047***	0.422
	pCO_2 (ppm)	square root	**0.001** ***	**0.031** *	**0.002** **	**0.039** *	0.373	0.337
Fig. S5	FCO_2 (mmol $m^{-2}d^{-1}$)	logarithmic (value+median)	**0.001** ***	0.238	**0.002** **	**0.018***	0.147	**0.041***
	FCH_4 (mmol $m^{-2}d^{-1}$)	logarithmic	**0.019***	**0.001*****	0.092	**0.001*****	**0.002****	0.124
	FN_2O (mmol $m^{-2}d^{-1}$)	logarithmic (value+median)	0.262	0.954	**0.028***	0.279	**0.047***	0.881
Figure or table	Variable	Transformation	p-values of the Betadisper test					
			Fall vs Winter	Fall vs Spring	Fall vs Summer	Winter vs Spring	Winter vs Summer	Spring vs Summer
Tab. S2	Temperature (°C)	logarithmic	0.689	0.515	0.093	0.987	0.121	0.093
	$\%O_2$ (%)	logarithmic	**0.005** **	0.381	0.127	0.068	0.134	0.503
	SRP (µmol L^{-1})	square root	0.102	0.858	**0.002** **	0.105	0.565	0.071
	P_{tot} (mg L^{-1})	square root	0.908	0.879	**0.001** ***	0.779	0.103	**0.002** **
	NH_4^+ (µmol L^{-1})	square root	0.143	0.138	0.629	0.942	0.439	0.397
	NO_2^- (µmol L^{-1})	square root	0.801	0.492	0.392	0.584	0.078	0.057
	NO_3^- (µmol L^{-1})	square root	0.412	0.665	0.852	0.614	0.364	0.596
	DIN (µmol L^{-1})	square root	0.407	0.722	0.912	0.624	0.523	0.829
	Chl-a (µg L^{-1})	square root	0.721	0.340	**0.001** ***	0.194	**0.002** **	**0.002** **
	TSM (mg L^{-1})	square root	0.933	0.814	0.159	0.799	**0.006** **	**0.004** **
Fig. 3	CH_4 (nmol L^{-1})	logarithmic	0.934	0.842	0.066	0.919	0.083	0.045
	$\%N_2O$ (%)	logarithmic	0.445	0.861	**0.022***	0.326	**0.026***	**0.031***
	pCO_2 (ppm)	square root	0.119	0.197	0.122	**0.049** **	0.059	0.417
Fig. S5	FCO_2 (mmol $m^{-2}d^{-1}$)	logarithmic (value+median)	0.903	0.064	0.031*	**0.019***	**0.017***	0.969
	FCH_4 (mmol $m^{-2}d^{-1}$)	logarithmic	0.928	0.508	0.084	0.566	0.075	0.095
	FN_2O (mmol $m^{-2}d^{-1}$)	logarithmic (value+median)	0.273	0.941	**0.046***	0.174	**0.036***	**0.027***

Table S6: Outcomes of the Betadisper and Permanova statistical tests for variables shown in box plots from the listed Figures. Comparisons marked with a square (■) are not shown in boxplots but were conducted using quantile regressions. These additional comparisons were performed to assess a statistical value of the dispersion, which is not provided in quantile regressions. Transformations have been applied to the data to ensure a normal distribution, and are indicated in the Transformation column.

	Variable	Transformation	Betadisper	Permanova
		Low (<40%) vs high (>40%) macrophyte cover		
Fig. 6	pCO_2 (ppm)	square root	0.641	0.136
	CH_4 (nmol L^{-1})	logarithmic	0.989	**0.005****
	$\%N_2O$ (%)	logarithmic	0.524	0.361
Fig. S3	Chl-a (µg L^{-1})	logarithmic	0.294	**0.003****
	P_{tot} (mg L^{-1})	none	0.833	0.975
	SRP (µmol L^{-1})	none	0.117	0.127
	Residence time (days)	none	0.263	0.144
	Distance (km)	logarithmic	0.63	**0.048***
	Surface (ha)	none	0.669	**0.041***
	DIN (µmol L^{-1})	square root	0.1472	**0.028***
		Natural (Holgerson and Raymond, 2016) vs Brussels ponds (This Study)		
Fig. 9	pCO_2 (µmol L^{-1})	logarithmic	0.125	**0.014***
	CH_4 (nmol L^{-1})	logarithmic	0.973	**0.001*****
		Center vs Periphery (■)		
None	$\%N_2O$ (%)	logarithmic	**0.02***	**0.003****
	DIN (µmol L^{-1})	square root	0.132	**0.041***
	NH_4^+ (µmol L^{-1})	square root	0.481	0.265
	NO_2^- (µmol L^{-1})	square root	0.125	**0.009****
	NO_3^- (µmol L^{-1})	square root	0.104	**0.007****
	pCO_2 (ppm)	square root	0.073	0.328
	CH_4 (nmol L^{-1})	logarithmic	0.573	**0.009****
		Small surfaces (<1ha) vs High Surfaces (>1ha) (■)		
None	$\%N_2O$ (%)	logarithmic	**0.03***	**0.012***
	DIN (µmol L^{-1})	square root	0.0953	**0.043***
	NH_4^+ (µmol L^{-1})	square root	0.11	**0.567**
	NO_2^- (µmol L^{-1})	square root	0.103	**0.037***
	NO_3^- (µmol L^{-1})	square root	0.107	**0.047***
	pCO_2 (ppm)	square root	0.128	**0.018***
	CH_4 (nmol L^{-1})	logarithmic	0.873	**0.011***

Table S7: Equation of quantiles regressions in listed figures and p-value (Wald test).

Figure	Database	Variable 1 (response)	Variable 2 (explicative)	Equation of quantile regression	p-value (Wald test)	Statistical significance
Fig. 4	All	pCO_2 (ppm)	$\%O_2$ (%)	$\sqrt{pCO_2} = 198.06 - 76.83 \times log(\%O_2)$	0.0000	****
			Temperature (°C)	$\sqrt{pCO_2} = 66.2 - 9.10 \times log(T)$	0.5400	ns
			Chl-a (µg L^{-1})	$\sqrt{pCO_2} = 64.14 - 2.18 \times \sqrt{Chla}$	0.1095	ns
			DIN (µmol L^{-1})	$\sqrt{pCO_2} = 45.42 + 1.40 \times \sqrt{DIN}$	0.1624	ns
			SRP (µmol L^{-1})	$\sqrt{pCO_2} = 24.37 + 22.60 \times \sqrt{SRP}$	0.0004	***
			P_{tot} (mg L^{-1})	$\sqrt{pCO_2} = 47.86 + 12.21 \times \sqrt{P_{tot}}$	0.4448	ns
		CH_4 (nmol L^{-1})	$\%O_2$ (%)	$log(CH_4) = 4.60 - 0.80 \times log(\%O_2)$	0.0124	*
			Temperature (°C)	$log(CH_4) = 2.22 + 0.91 \times log(T)$	0.0000	****
			Chl-a (µg L^{-1})	$log(CH_4) = 3.26 - 0.04 \times \sqrt{Chla}$	0.0296	*
			DIN (µmol L^{-1})	$log(CH_4) = 3.52 - 0.04 \times \sqrt{DIN}$	0.0069	**
			SRP (µmol L^{-1})	$log(CH_4) = 3.06 + 0.02 \times \sqrt{SRP}$	0.8903	ns
			P_{tot} (mg L^{-1})	$log(CH_4) = 2.67 + 0.63 \times \sqrt{P_{tot}}$	0.0000	****
		$\%N_2O$ (%)	$\%O_2$ (%)	$log(\%N_2O) = 2.78 - 0.33 \times log(\%O_2)$	0.0488	*
			Temperature (°C)	$log(\%N_2O) = 2.36 - 0.21 \times log(T)$	0.0356	*
			Chl-a (µg L^{-1})	$log(\%N_2O) = 2.13 + 0.01 \times \sqrt{Chla}$	0.6087	ns
			DIN (µmol L^{-1})	$log(\%N_2O) = 1.88 + 0.04 \times \sqrt{DIN}$	0.0000	****
			SRP (µmol L^{-1})	$log(\%N_2O) = 1.96 + 0.15 \times \sqrt{SRP}$	0.0956	ns
			P_{tot} (mg L^{-1})	$log(\%N_2O) = 2.21 - 0.07 \times \sqrt{P_{tot}}$	0.2153	ns
Fig. 5			NH_4^+ (µmol L^{-1})	$log(\%N_2O) = 2.06 + 0.03 \times \sqrt{(NH_4^+)}$	0.0436	*
			NO_3^- (µmol L^{-1})	$log(\%N_2O) = 1.91 + 0.04 \times \sqrt{NO_3^-}$	0.0000	****
			NO_2^- (µmol L^{-1})	$log(\%N_2O) = 1.84 + 0.36 \times \sqrt{NO_2^-}$	0.0000	****
			O_2:DIN (mol:mol)	$log(\%N_2O) = 2.41 - 0.35 \times log(O_2{:}DIN)$	0.0001	****
			O_2: NH_4^+ (mol:mol)	$log(\%N_2O) = 2.27 - 0.07 \times log(O_2{:}NH_4^+)$	0.1007	ns
			O_2: NO_3^- (mol:mol)	$log(\%N_2O) = 2.46 - 0.31 \times log(O_2{:}NO_3^-)$	0.0001	****
			O_2: NO_2^- (mol:mol)	$log(\%N_2O) = 2.94 - 0.32 \times log(O_2{:}NO_2^-)$	0.0001	****
Fig. 6	Average for each pond	pCO_2 (ppm)	Surface (ha)	$\sqrt{pCO_2} = 68.64 - 6.74 \times Surface$	0.0020	**
			Distance (km)	$\sqrt{pCO_2} = 57.64 - 0.23 \times Distance$	0.9203	ns
		CH_4 (nmol L^{-1})	Surface (ha)	$log(CH_4) = 3.18 + 0.13 \times Surface$	0.0168	*
			Distance (km)	$log(CH_4) = 2.92 + 0.08 \times Distance$	0.0036	**
		$\%N_2O$ (%)	Surface (ha)	$log(\%N_2O) = 2.36 - 0.12 \times Surface$	0.0479	*
			Distance (km)	$log(\%N_2O) = 2.73 - 0.09 \times Distance$	0.0081	**
Fig. S2	Fall	CH_4 (nmol L^{-1})	P_{tot} (mg L^{-1})	$log(CH_4) = 1.99 + 1.35 \times \sqrt{P_{tot}}$	0.0273	*
	Winter			$log(CH_4) = 2.87 - 0.09 \times \sqrt{P_{tot}}$	0.8880	ns
	Spring			$log(CH_4) = 2.29 + 0.46 \times \sqrt{P_{tot}}$	0.0123	*
	Summer			$log(CH_4) = 2.55 + 0.38 \times \sqrt{P_{tot}}$	0.0038	**
	Fall		DIN (µmol L^{-1})	$log(CH_4) = 3.07 + - 0.01 \times \sqrt{DIN}$	0.8728	ns
	Winter			$log(CH_4) = 2.92 - 0.01 \times \sqrt{DIN}$	0.6101	ns
	Spring			$log(CH_4) = 3.86 - 0.07 \times \sqrt{DIN}$	0.0080	**
	Summer			$log(CH_4) = 3.43 + 0.01 \times \sqrt{DIN}$	0.9405	ns
	Fall	$\%N_2O$ (%)		$log(\%N_2O) = 1.78 + 0.05 \times \sqrt{DIN}$	0.0005	***
	Winter			$log(\%N_2O) = 1.90 + 0.03 \times \sqrt{DIN}$	0.0000	****
	Spring			$log(\%N_2O) = 1.86 + 0.06 \times \sqrt{DIN}$	0.0071	**
	Summer			$log(\%N_2O) = 1.77 + 0.08 \times \sqrt{DIN}$	0.0317	*
Fig. 7	Average for each pond	DIN (µmol L^{-1})	Distance (km)	$\sqrt{DIN} = 13.25 - 0.98 \times Distance$	0.0294	*
		NH_4^+ (µmol L^{-1})		$\sqrt{(NH_4^+)} = 2.27 + 0.33 \times Distance$	0.3210	ns
		NO_3^- (µmol L^{-1})		$\sqrt{NO_3^-} = 15.22 - 1.45 \times Distance$	0.0015	**
		NO_2^- (µmol L^{-1})		$\sqrt{NO_2^-} = 2.01 - 0.16 \times Distance$	0.0311	*
		atm NO_2^- (µg m^{-3})		$atm\ NO_2^- = 37.56 - 3.35 \times \mathrm{Distance}$	0.0003	***
		$\%N_2O$ (%)	atm NO_2^- (µg m^{-3})	$\log(\%N_2O) = 1.66 + 0.04 \times \mathrm{atm}\ NO_2^-$	0.0043	**
Fig. S4		Chl-a (µg L^{-1})	Distance (km)	$\sqrt{\mathrm{Chla}} = 1.61 - 0.05 \times \mathrm{Distance}$	0.3410	ns